

1 Title: Equivalent noise characterization of human lightness constancy
2 Authors: Vijay Singh^{1,2}, Johannes Burge^{2,3,4,5}, David H. Brainard^{2,3,4,5}
3 1 Department of Physics, North Carolina Agricultural and Technical State University, Greensboro, NC,
4 USA.
5 2 Computational Neuroscience Initiative, University of Pennsylvania, Philadelphia, PA, USA.
6 3 Department of Psychology, University of Pennsylvania, Philadelphia, PA, USA.
7 4 Neuroscience Graduate Group, University of Pennsylvania, Philadelphia, PA, USA.
8 5 Bioengineering Graduate Group, University of Pennsylvania, Philadelphia, PA, USA.

9
10
11 **ABSTRACT:** A goal of visual perception is to provide stable representations of task-relevant scene
12 properties (e.g. object reflectance) despite variation in task-irrelevant scene properties (e.g. illumination,
13 reflectance of other nearby objects). To study such stability in the context of the perceptual representation
14 of lightness, we introduce a threshold-based psychophysical paradigm. We measure how thresholds for
15 discriminating the achromatic reflectance of a target object (task-relevant property) in rendered
16 naturalistic scenes are impacted by variation in the reflectance functions of background objects (task-
17 irrelevant property), using a two-alternative forced-choice paradigm in which the reflectance of the
18 background objects is randomized across the two intervals of each trial. We control the amount of
19 background reflectance variation by manipulating a statistical model of naturally-occurring surface
20 reflectances. For low background object reflectance variation, discrimination thresholds were nearly
21 constant, indicating that observers' internal noise determines threshold in this regime. As background
22 object reflectance variation increases, its effects start to dominate performance. A model based on signal
23 detection theory allows us to express the effects of task-irrelevant variation in terms of the equivalent
24 noise, that is relative to the intrinsic precision of the task-relevant perceptual representation. The results
25 indicate that although naturally-occurring background object reflectance variation does intrude on the
26 perceptual representation of target object lightness, the effect is modest - within a factor of two of the
27 equivalent noise level set by internal noise.

28
29
30 **KEYWORDS:** Lightness, Noise Masking, Equivalent Noise, Human Psychophysics, Color Vision

31
32
33
34
35
36

37 **INTRODUCTION**

38
39 To support effective action, vision provides stable perceptual representations of the distal properties of
40 objects. The computations that give rise to these representations start with the information in the proximal
41 stimuli that are encoded by the retinas. These proximal stimuli depend on the intrinsic properties of the
42 objects in the scene, on object-extrinsic properties of the scene (e.g. illumination), and on the observer's
43 particular viewpoint. A challenge for the visual system is to recover stable perceptual correlates of object-
44 intrinsic properties across variation in other scene variables. Understanding the degree to which the visual
45 system rises to this challenge, and how it does so, is an important goal of vision science (Helmholtz,
46 Knill & Richards, 1996; Brascamp & Shevell, 2021; Geisler, 2008; Burge, 2020; Wandell &
47 Brainard, in press).

48
49 Here we consider the perceptual task of representing the reflectance of an object embedded in a scene,
50 based on the light reflected to the eye from the object and the rest of the scene. The perceptual correlate of
51 object surface reflectance is its perceived color or, in the special case of achromatic objects, its lightness.
52 Computing a stable color or lightness representation poses a challenge to the visual system because the
53 retinal image of the object varies with the object's reflectance, the spectral irradiance of the illumination,
54 the position and pose of the object in the scene, and the properties of other objects in the scene. The
55 degree to which the visual system succeeds at stabilizing its color and lightness representations of objects,
56 in the face of variation extrinsic to their reflectance, determines the degree to which the visual system
57 achieves color and lightness constancy.

58
59 Under many circumstances, the visual system achieves a high degree of color and lightness constancy
60 (Foster, 2011). Several theoretical frameworks have been developed to account for this ability. The
61 frameworks attempt to explain how different cues are processed to form stable perceptual representations
62 of object reflectance (Adelson, 2000; Smithson, 2005; Gilchrist, 2006; Kingdom, 2011; Foster, 2011;
63 Brainard & Maloney, 2011; Brainard & Radonjić, 2014; Witzel & Gegenfurtner, 2018; Hurlbert, 2019;
64 Murray, 2021). The underlying computations have been explained in terms of mechanistic gain control
65 (e.g., von Kries, 1905; Whittle & Challands, 1969; Webster & Mollon, 1995; Land & McCann, 1971;
66 Horn, 1974), cue combination (e.g., Maloney & Yang, 2001; Yang & Maloney, 2001), Bayesian inference
67 (e.g., Brainard & Freeman, 1997; Brainard et al., 2006; Barron & Malik, 2012a; Allred & Brainard, 2013;
68 Murray, 2020; see also Boyaci, Maloney, & Hersh, 2003; Bloj et al., 2004; Brainard & Maloney, 2011),
69 learned computations (e.g., Singh, Cottaris, Heasly, Brainard, & Burge, 2018; Flachot & Gegenfurtner,
70 2018; Flachot & Gegenfurtner, 2021; Afifi, Barron, LeGendre, Tsai, & Bleibel, 2021), and application of
71 principles of perceptual organization (Gilchrist, 2006; Adelson, 1993).

72
73 Color constancy and lightness constancy have been elucidated primarily with an experimental approach in
74 which observers report on suprathreshold aspects of the color or lightness of a target object, across
75 changes extrinsic to the target object's reflectance.¹ In these experiments, the target object's reflectance is
76 the task-relevant scene variable, while other aspects of the scene are task irrelevant. Observers' reports
77 are solicited using a variety of methods, including matching (e.g., Burnham, Evans, & Newhall, 1952;
78 Gilchrist, 1977; Arend & Reeves, 1986; Brainard, Brunt, & Speigle, 1997), naming (e.g., Helson &
79 Jeffers, 1940; Olkkonen, Witzel, Hansen, & Gegenfurtner, 2010), scaling (e.g., Schultz, Doerschner, &
80 Maloney, 2006), and nulling (e.g., Helson & Michels, 1948; Jameson & Hurvich, 1955; Chichilnisky &
81 Wandell, 1997; Brainard, 1998).

¹ This type of experiment may be instrumented with instructions that prompt the observer to report how the object appears, or with instructions that prompt the subject to report their estimate of some aspect of the object's reflectance. Exactly what observers report under either of these instructional regimes, as well as the nature of instructional effects, is an important but thorny issue that we will not digress on further in this paper. See Radonjić and Brainard (2016) for a recent treatment of the issue, as well as the references therein.

82
83 In the study of perception, discrimination experiments complement experiments that rely on
84 suprathreshold reports. In a typical discrimination experiment, observers choose which of two stimuli has
85 a larger physical value along some stimulus dimension. The stimulus difference is titrated to determine
86 the smallest change that supports criterion discrimination performance. This smallest change is defined as
87 threshold. For example, observers might be tasked with reporting which of two objects has a larger
88 lightness value, in an effort to determine the human ability to discriminate different object surface
89 reflectances. Mature theory links discrimination thresholds to the precision of the underlying perceptual
90 representation (Green, 1966). Theory also exists for linking thresholds to properties of neural responses
91 (Brindley, 1960; Green, 1966; Teller, 1984; Parker & Newsome, 1998).

92
93 Theory is less well developed for how to use discrimination experiments to address questions about
94 perceptual constancy. In the case of color constancy, one approach is to measure observers' ability to
95 discriminate changes in scene illumination (Pearce, Crichton, Mackiewicz, Finlayson, & Hurlbert, 2014;
96 Radonjić et al., 2016; Radonjić et al., 2018; Aston, Radonjić, Brainard, & Hurlbert, 2019; Alvaro,
97 Linhares, Moreira, Lillo, & Nascimento, 2017), rather than to measure the ability to detect a change in
98 object surface reflectance per se (for work that measures reflectance discrimination thresholds see
99 Morimoto & Smithson, 2018). The idea is that if illumination changes are subthreshold, then the
100 perceptual representations of both surface reflectance and illumination are stable across those illumination
101 changes. However, it is unclear how the results of these experiments connect to and inform us about the
102 stability of perceptual judgments across the larger illumination changes that occur in natural viewing (but
103 see Weiss, Witzel, & Gegenfurtner, 2017). Another approach is to link discrimination thresholds to
104 suprathreshold reports of perceived stimulus properties, an approach which has its origins in Fechner's
105 pioneering interpretation of Weber's Law (Fechner, 1860). The idea is that both threshold and
106 suprathreshold percepts are mediated by a common stimulus-response function whose properties depend
107 on, and change with, viewing context. Although positing a common stimulus-response function holds
108 promise (Nachmias & Sansbury, 1974; Hillis & Brainard, 2005; Hillis & Brainard, 2007b), there are cases
109 in which the discrimination thresholds do not predict suprathreshold measures of lightness constancy
110 made using well-matched stimuli (Hillis & Brainard, 2007a).

111
112 Here, we introduce a new approach to using discrimination experiments to study perceptual constancy.
113 The approach is based on measuring how discrimination thresholds for a task-relevant scene property are
114 affected by variation in a task-irrelevant scene property. The approach is conceptually similar to studying
115 how contrast thresholds are affected by addition of random, unpredictable stimulus variation, usually
116 introduced in the form of spatially white or pink contrast noise (Legge, Kersten, & Burgess, 1987; Pelli,
117 1990; Pelli & Farell, 1999). It is conceptually distinct in that the random, unpredictable variation is
118 introduced in the distal scene properties (for related recent work, see Zhu, Yuille, & Kersten, 2021). We
119 apply this approach to the study of lightness constancy in naturalistic scenes. First, we measure human
120 ability to discriminate the achromatic surface reflectance of a target object in the absence of any target
121 object-extrinsic variation. Next, we measure how these lightness discrimination thresholds change with
122 the introduction of target object-extrinsic variation. Specifically, we introduce random, unpredictable
123 variation to the background objects in the scene by varying their reflectance spectra—loosely, their colors
124 (Lotto & Purves, 1999; Brown & MacLeod, 1997). The lightness discrimination threshold at each level of
125 background object reflectance variation measures how difficult the lightness discrimination task is for that
126 level of variation. The change in difficulty from baseline (i.e., no background object reflectance variation)
127 quantifies the degree to which the background variation intrudes on the perceptual representation of target
128 lightness.

129
130 As the variation in background object reflectances is increased, we find that discrimination thresholds are
131 initially constant and then increase. To interpret these findings, we develop a model based on signal
132 detection theory; the model is similar to those used to understand the effect of contrast noise on contrast

133 thresholds (Legge, Kersten, & Burgess, 1987; Pelli, 1990). The model relates thresholds for the task-
134 relevant variable (here, target object reflectance) to the amount of variation in the task-irrelevant variable
135 (here, background object reflectance). The model allows us to express the effect of task-irrelevant
136 variation in terms of equivalent noise. Equivalent noise is the amount of external task-irrelevant variation
137 whose effect on the perceptual representation is the same as that of internal noise. We find that the
138 intrusion of naturally occurring variation in background object reflectances on the perceptual
139 representation of lightness is within a factor of two of the equivalent noise.

140
141 The paper is organized as follows: Section 2 (Methods) provides the experimental methods. Section 3
142 (Model) introduces the model used to interpret the data, and discusses the concept of equivalent noise in
143 more detail. Section 4 (Results) reports the experimental results in the context of the model. Section 5
144 (Discussion) provides a summary. The Appendix describes a control experiment and provides
145 supplemental figures and tables. Additional supplementary information is available online as indicated in
146 Methods: Code and Data Availability.

147 **2 EXPERIMENTAL METHODS**

148 **Overview**

149 We studied the effect of variability in object-extrinsic properties on the human ability to discriminate an
150 object-intrinsic property. Specifically, we measured how variation in the reflectance spectra of
151 background objects affects lightness discrimination thresholds, that is thresholds for discriminating object
152 achromatic reflectance.² We used a two-alternative forced-choice (2AFC) procedure (Figure 1). On each
153 trial, observers viewed a standard image and comparison image, sequentially presented on a calibrated
154 monitor for 250ms each. The inter-stimulus interval was 250ms (Figure 1a). The images were computer
155 graphics renderings of 3D scenes. Each scene contained a spherical target object that appeared
156 achromatic. The observers' task was to report the image in which the target object was lighter. Across
157 trials, we varied the luminous reflectance factor (LRF; American Society for Testing and Materials, 2017)
158 of the target object in the comparison image while keeping the LRF of the target object in the standard
159 image fixed. The LRF is the ratio of the luminance of a surface under a reference illuminant (here, the
160 CIE D65 reference illuminant) to the luminance of the reference illuminant itself. The target object LRF
161 was varied by scaling the surface reflectance spectrum of the target object, without changing its shape.³
162 The temporal order in which the standard and comparison images were presented was randomized on
163 each trial.

164
165 We recorded the proportion of times observers chose the comparison image as having the lighter target
166 object at 11 values of the target object LRF. Figure 2 shows a psychometric function from a typical
167 human observer. The proportion-comparison-chosen data were fit with a cumulative normal using
168 maximum likelihood methods (see Methods: Psychometric Function). Threshold was defined as the
169 difference between the LRF of the target object at proportion comparison chosen 0.76 and 0.50 (i.e., d-
170 prime = 1.0 in a two-interval task), as determined from the cumulative normal fit.

² We adopt the lightness discrimination threshold terminology based on the underlying assumption that observers perform the task using their perceptual lightness representation, and indeed our instructions to subjects used the lightness terminology to describe what should be judged. The actual stimulus variable being varied, however, was the simulated achromatic reflectance of the target object being judged, and feedback was given based on the value of this reflectance. In this paper, we do not explore the question as to whether the results would be affected if we had varied the instructions given to subjects (see footnote 1 above).

³ We use LRF rather than the more generic term albedo as our single number summary of the underlying spectral surface reflectance function, as the LRF is explicit about how variation in reflectance over wavelength should be taken into account.

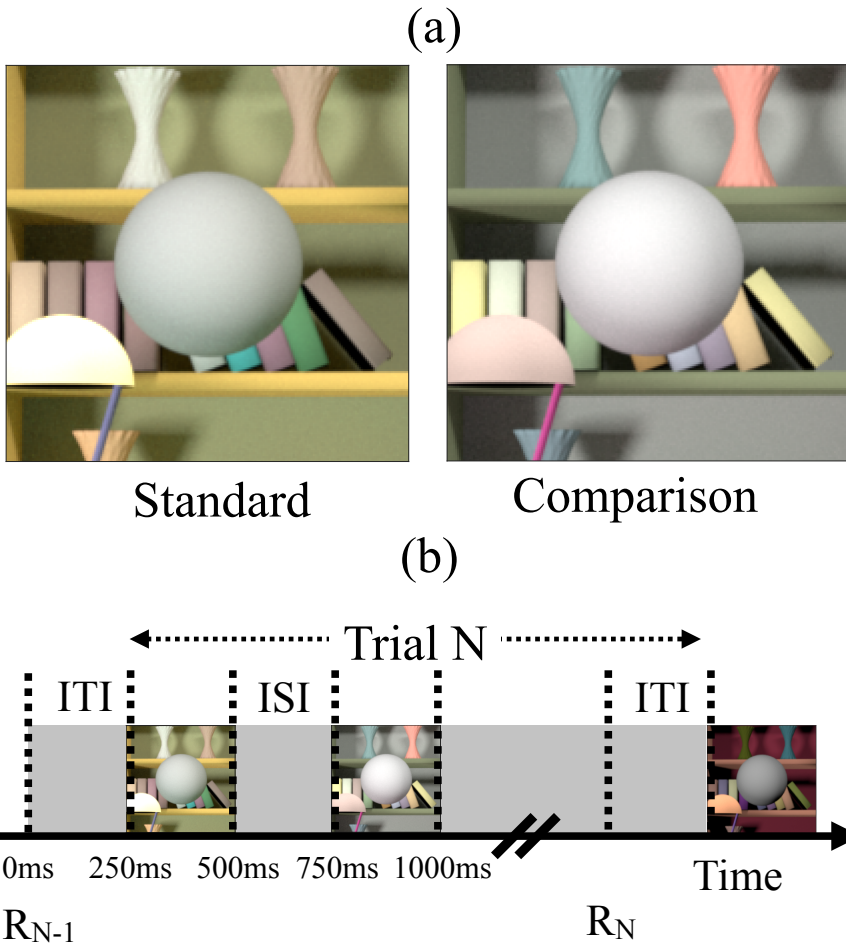


Figure 1: Psychophysical task. (a) On every trial of the experiment, human observers viewed two images in sequence, a standard image and a comparison image and indicated the one in which the spherical target object in the center of the image was lighter. Example standard and comparison images are shown. The images were computer graphics simulations. The simulated reflectance functions of the target were spectrally flat, and the spheres appeared gray. The overall reflectance of the target was held fixed in the standard images and differed between standard and comparison. Performance (proportion correct) was measured as a function of this difference to determine discrimination threshold. The reflectance spectra of objects in the background could be held fixed or vary between standard and comparison on each trial (as illustrated here). The order of presentation of the standard and comparison images was randomized from trial to trial. Discrimination thresholds were measured as function of the amount of variation in background object reflectances. (b) Trial sequence. R_{N-1} indicates the time of the observer's response for the $(N-1)^{\text{th}}$ trial. The N^{th} trial begins 250ms after that response (Inter Trial Interval, ITI). The N^{th} trial consists of two 250ms stimulus presentation intervals with a 250ms inter-stimulus interval (ISI). The observer responds by pressing a button on a gamepad after the second stimulus has been shown. The observer can take as long as he or she wishes before making the response, with an example response time denoted by R_N in the figure. The next trial begins 250ms after the response.

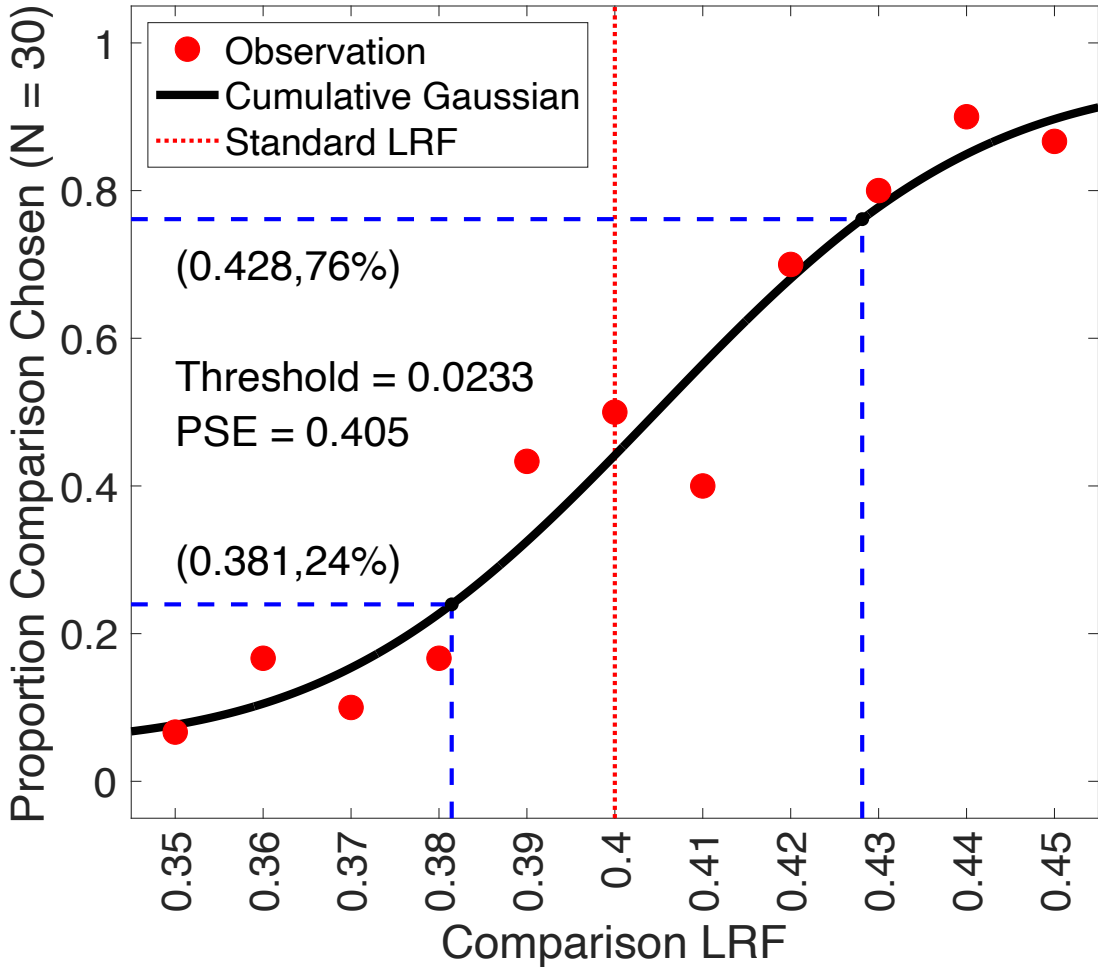


Figure 2: Psychometric function. We recorded the proportion of times the observer chose the target in the comparison image to be lighter, as a function of the comparison LRF. The LRF of the target object in the standard image was fixed at 0.4. The LRF of the target object in the comparison image were chosen from 11 linearly spaced values in the range [0.35, 0.45]. In each block, thirty trials were presented at each comparison LRF value. We fit a cumulative normal distribution to the proportion comparison chosen data using maximum likelihood methods. The guess and lapse rates were constrained to be equal and were restricted to be in the range [0, 0.05]. The threshold was measured as the difference between the LRF at proportion comparison chosen equal to 0.76 and 0.5, as predicted by the cumulative normal fit. This figure shows the data for Observer 2 for scale factor 0.00, for the block run in the first experimental session for that observer. The point of subjective equality (PSE, the LRF corresponding to proportion chosen 0.5) was close to 0.4 as expected and the threshold was 0.0233. The lapse rate for this fit was 0.05.

171
172 We measured lightness discrimination thresholds as a function of the amount of variability in the surface
173 reflectances of the background objects in the rendered scenes. The reflectances of the background objects
174 were chosen from a distribution of natural reflectances. The amount of variability was controlled
175 parametrically by multiplying the covariance matrix of the distribution by a scalar (see Methods:
176 Reflectance and Illumination Spectra). We measured thresholds for six logarithmically spaced values of
177 this covariance scalar. By varying the scalar from 0 (no variation) to 1 (natural-scene-typical variation),
178 we examined how background variation affects performance in the task. Figure 3 shows examples of
179 images used in our psychophysical task for different choices of the covariance scalar.

180 The subsections below provide additional methodological detail.

181 **Preregistration**

182 The experimental design and the method for extracting threshold from the data were preregistered before
183 the start of the experiment. The preregistration documents are publicly available at: <https://osf.io/7tgy8/>.⁴

184 We preregistered three experiments. The first experiment (preregistered as Experiment 1) was abandoned
185 because the task was too difficult. The findings of the second experiment (preregistered as Experiment 2
186 and referred to here as the control experiment) provide control data and are reported in the Appendix. In
187 the body of the paper, we report preregistered Experiment 3 (referred to here as the main experiment).
188 The details of the experimental methods below refer to preregistered Experiment 3; the methods for
189 preregistered Experiment 2 were essentially the same with key differences (primarily the conditions
190 studied) described in the Appendix.

191 A deviation from the preregistered plan for preregistered Experiment 2 was the change in the criteria to
192 select observers for the experiment. The preregistered criterion for selecting an observer for this
193 experiment was that an observer would be excluded if their mean threshold for the last two blocks in the
194 practice session exceeded 0.025. After collecting data from 8 naive observers, we concluded that this
195 criterion was too strict as only one observer met the criterion. Hence, we increased exclusion threshold
196 from 0.025 to 0.030. The preregistered plans also indicated that each image would be presented for
197 500ms, but in the event we shortened this to 250ms.

198 We followed the procedure described in the preregistration document to extract threshold from the data.
199 The document also indicated that the primary data feature of interest was the dependence of threshold on
200 the covariance scalar and predicted that thresholds would increase with increasing background variability.
201 The quantitative models of the data, however, were developed post-hoc.

202 **Reflectance and Illumination Spectra**

203 The reflectance spectra for the background objects in the scene were generated using a model of naturally
204 occurring surface reflectance spectra, as described in (Singh, Cottaris, Heasly, Brainard, & Burge, 2018).
205 Briefly, we started with two datasets of surface reflectance functions (Kelly, Gibson, & Nickerson, 1943;
206 Vrhel, Gershon, & Iwan, 1994) containing 632 surface reflectance measurements in total. The Kelly et al.
207 dataset has 462 spectral measurements of Munsell papers, with each spectrum available to us
208 (psychtoolbox.org) on wavelength support 400nm to 700nm at 5nm spacing. The Vrhel dataset has 170
209 spectral measurements, each spectrum measured in the wavelength range 390nm to 730nm at 2nm

⁴ The preregistration documents relevant to this paper are those for Experiments 1, 2 and 3. The site also contains preregistrations for subsequent work not reported in this paper.

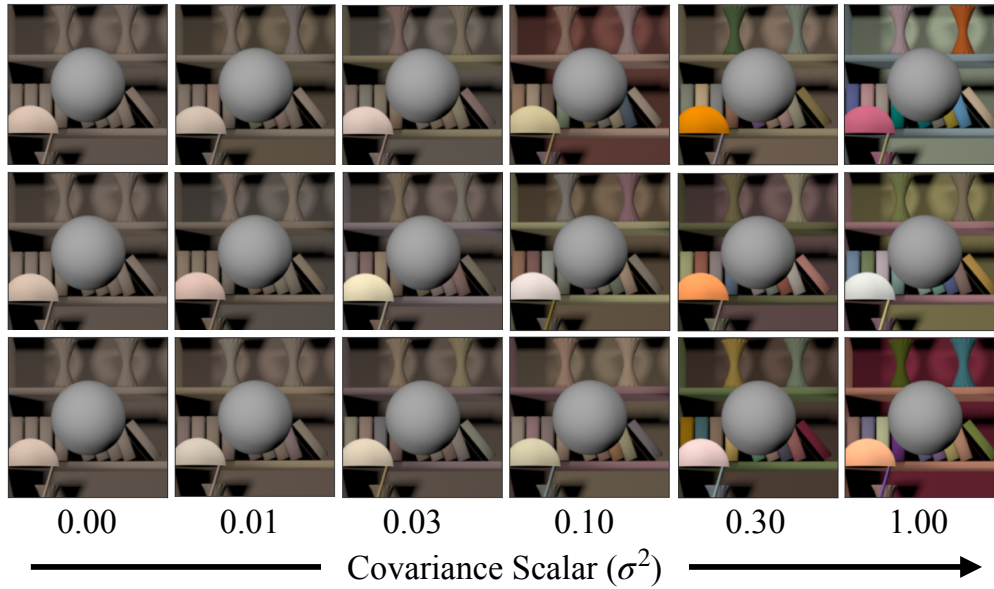


Figure 3: Variation in background object reflectances: The reflectance spectra of background objects were chosen from a multivariate normal distribution that modeled the statistics of natural reflectance spectra. The variation in the reflectance spectra was controlled by multiplying the covariance matrix of the distribution with a scalar. We generated images at six levels of the scalar. Each column shows three sample images at each of the six values of the scalar. The leftmost column corresponds to no variation and the rightmost column corresponds to the modeled variation of natural reflectances. The target object (sphere at the center of each panel) in each image has the same LRF. For each value of the scalar, we generated 1100 images, 100 each at 11 linearly spaced target LRF levels across the range [0.35, 0.45]. Discrimination thresholds were measured separately for each value of the covariance scalar.

spacing. We converted to a common wavelength support of 10 nm spacing between 400nm and 700nm and combined the two datasets. We then used principal component analysis (PCA) to characterize the combined dataset. For this analysis, we mean centered the dataset and used the singular value decomposition (SVD) to obtain the eigenvectors of the mean-centered dataset. The reflectances in the mean-centered dataset were projected onto the eigenvectors to obtain their projection weights. The eigenvectors associated with the six largest eigenvalues captured more than 99.5% of the variance, so the rest of the analysis focuses on the projection weights on these eigenvectors. We approximated the empirical distribution of projection weights by a multivariate normal distribution. Reflectance spectra for the objects in the scene were generated by randomly sampling from this multivariate normal distribution and using the eigenvectors to construct samples of mean-centered surface reflectances. To these, we added back the mean of the surface reflectance dataset. We imposed a physical realizability constraint on the randomly generated spectral samples by ensuring that the reflectance at each wavelength was between 0 and 1. If the reflectance of a generated sample did not fall in this range at any wavelength, it was discarded.

The amount of variation in the surface reflectance of the background objects was controlled by multiplying the covariance matrix of the multivariate normal distribution (see above) by a covariance scalar. A covariance scalar of 0 corresponds to no background object reflectance variation. A covariance scalar of 1 corresponds to the full reflectance variation of the model of natural reflectance (Figure 3). We generated images for six logarithmically spaced values of covariance scalar: [0, 0.01, 0.03, 0.1, 0.3, 1.0]. Due to the physical realizability constraint, the actual variances of the projection weights for the generated spectral samples for some covariance scalars were lower than the corresponding variances of the underlying multivariate normal, and their distribution was not precisely multivariate normal.

The power spectrum of the light sources was chosen as that of standard daylight D65. We normalized the D65 spectrum by its mean power to obtain its relative spectral shape. This was multiplied by a fixed scalar with an arbitrarily chosen value of 5 to get the illuminant spectrum. This spectrum was used for all light sources in the visual scene and was not varied across the experiments reported here.

Image Generation

The images were generated using software we refer to as Virtual World Color Constancy (VWCC) (github.com/BrainardLab/VirtualWorldColorConstancy). VWCC is written using MATLAB. It harnesses the Mitsuba renderer (Jakob, 2010) to render simulated images from scene descriptions, and also takes advantage of our RenderToolbox package (rendertoolbox.org; Heasly, Cottaris, Lichtman, Xiao, & Brainard, 2014). To render an image, we first create a 3D model that specifies the base scene. Objects and light sources can be inserted in the base scene at user specified locations. The 3D models utilized a base scene provided as part of RenderToolbox and modified using Blender, an open-source 3-D modeling and animation package (blender.org). Next, we assigned reflectance spectra and spectral power distribution functions to the objects and light sources in the scene (see Methods: Reflectance and Illumination Spectra). For each image, reflectances were assigned to the background objects by random draw from the reflectance model described above, with appropriate covariance scale factor. This procedure means that a set of images embodies the variation in background spectra described by the reflectance model, with each individual image containing a variety of background reflectances (Figure 3). Illumination spectra were not varied throughout the experiments reported here, and illumination spectra were as described in Methods: Reflectance and Illumination Spectra above.

Once the geometrical and spectral features were specified, we rendered a 2D multispectral image of the scene using Mitsuba, a physically-realistic open-source rendering system (mitsuba-renderer.org; Jakob, 2010). The images were rendered at 31 wavelengths equally spaced between 400nm and 700nm. The images were rendered with the camera field of view of 17° with an image resolution of 320-pixel by 240-

258 pixels with the target object at the center. A 201-pixel by 201-pixel area, centered around the spherical
259 target object, was cropped for display on the monitor.
260

261 To present the multispectral images on the monitor, they were first converted to LMS images using the
262 Stockman-Sharpe 2° cone fundamentals (*T_cones_ss2* in the Psychophysics Toolbox). Then the monitor
263 calibration data and standard methods (Brainard, 1989; Brainard, Pelli, & Robson, 2002) were used to
264 convert the LMS images to gamma corrected RGB images. A common scaling was applied to all images
265 before rendering to ensure that they were within monitor gamut, so that the maximum linear channel RGB
266 channel input was 0.9. The gamma corrected RGB images was presented on the monitor during the
267 experiment.

268 **Stimulus Design**

269 As noted above, we measured lightness discrimination thresholds for six values of the covariance scalar.
270 For each value of the covariance scalar, we generated a dataset of 1100 images. The dataset had 100
271 images each at 11 values of the target object LRF. The LRF of the target object in the standard images
272 was 0.4 and the LRF in the comparison image varied between 0.35 and 0.45 at steps of 0.01 (11
273 comparison levels). We generated 100 images at each comparison level, each with a different choice of
274 the reflectance spectra of the background objects. The fact that we had 100 images for each target LRF
275 allowed us to randomize the background object reflectances across the two intervals of each forced choice
276 trial without excessive replication. For covariance scalar 0.00 we generated a set of 11 images, one at
277 each LRF level, as the background remained fixed in this case. All images were generated without
278 secondary reflections specified in the rendering process. The geometry of the 3D scene was also held
279 fixed across all images.
280

281 When displayed on the experimental monitor, the average luminance of the standard image for covariance
282 scalar 0.00 was 47.3 cd/m². The average luminances of the target object for the 11 LRF levels were [67.0,
283 68.0, 68.9, 69.8, 70.7, 71.6, 72.5, 73.4, 74.2, 75.1, 75.9] cd/m².
284

285 **Experimental Details**

286 We define a trial as the presentation of two images (standard and comparison images) and collection of
287 the observer's response. We define an interval as the presentation of one of the images in the trial.
288

289 The experiment was structured as follows. We define a block of trials as the data collected at one
290 covariance scalar with 30 trials at each of the 11 comparison levels. We define a permutation as a set of
291 six blocks, where each block corresponds to one of the possible six covariance scalars. We collected three
292 permutations for each observer, with a new random order drawn for each permutation. Thus, after the
293 practice session (see Methods: Observer Recruitment and Exclusion), there were total 18 blocks. We
294 divided these 18 blocks over 6 sessions, each session with 3 blocks. In each block, we randomly selected
295 the images for the trials from the pre-generated image database. The first five trials of each block were
296 moderate trials (as defined in Methods: Observer Recruitment and Exclusion) to acclimatize the observer
297 to the experimental task. The responses for these five trials were not saved.
298

299 The trial sequence (comparison level, specific images, standard/comparison order) in a block was
300 generated pseudo-randomly at the beginning of the block. For this, at each comparison lightness level, 30
301 standard and comparison images were chosen pseudo-randomly with replacement from the image dataset.
302 The sequence of presentation of these 330 trials were randomized and saved. For each trial, the order of
303 presentation of the standard and comparison image was also determined pseudo-randomly and saved. The
304 trials were presented according to the saved sequence.

305
306 The trials in a block were presented in three sub-blocks of 110 trials each. At the end of each sub-block
307 the observer took a break of minimum duration 1 minute. The observer could terminate the experiment
308 anytime during the block. If an observer terminated a block, the data for that block was not saved. No
309 observer terminated any block. One observer indicated a desire to postpone at the beginning of a session,
310 due to fatigue for reasons unrelated to the experiment. The session was rescheduled.
311

312 At the beginning of the first experimental session (the practice session) for each observer, the
313 experimenter explained the experimental procedures and obtained consent for the experiments. The
314 experimenter then tested the observer for normal visual acuity and color vision. The observer was then
315 taken to the experimental room, where the experimenter described the task, and the observer was shown
316 the display, chin rest, and response box. The observer was dark adapted by sitting in the dark room for
317 approximately 5 minutes. The observer then performed the familiarization block (see Methods: Observer
318 Recruitment and Exclusion for explanation of familiarization block). After the familiarization block, the
319 observer performed the other three blocks of the practice session. The practice session lasted about one
320 hour.

321 Observers who met the inclusion criteria (see Methods: Observer Recruitment and Exclusion) then
322 performed 18 blocks over 6 additional sessions, each on a separate day. The order of blocks for each
323 observer was determined pseudo-randomly at the beginning of the practice session. As noted above,
324 observers performed three blocks per session. Observers were dark adapted for 5 minutes at the beginning
325 of each session. The data for all observers in the main experiment (preregistered Experiment 3) were
326 collected over a period of four weeks.
327

328 Observers viewed the stimuli with both eyes.
329

330 **Observer Recruitment and Exclusion**

331
332 Observers were recruited from the University of Pennsylvania and the local Philadelphia community and
333 were compensated for their time. Observers were screened to have normal visual acuity (20/40 or better;
334 with corrective eyewear, if applicable) and normal color vision, as assessed with pseudo-isochromatic
335 plates (Ishihara, 1977). These exclusion criteria were specified in the preregistration document (see
336 Methods: Preregistration). One observer was discontinued at this point for not meeting the normal visual
337 acuity criterion.
338

339 Observers who passed the vision screening then participated in a practice session. This session also served
340 to screen for observers' ability to reliably perform the psychophysical task. At the beginning of the
341 practice session, observers were familiarized with the task via a familiarization block. In the
342 familiarization block, observers performed 40 trials of the task using images with covariance scalar 0.00
343 (10 easy trials, 10 moderate trials, and 20 regular trials). In the easy trials, the observers compared images
344 with target object LRF 0.35 and 0.45. In the moderate trials, they compared images with target object
345 LRF 0.40 to images with target object LRF 0.35 or 0.45. In the regular trials they compared images with
346 target object LRF 0.40 to images with target object LRF in the range [0.35, 0.45]. The data from the
347 familiarization block was not saved. The observer then performed three normal blocks for images with
348 covariance scalar 0.00. At the end of the practice session, the mean threshold of the observer for the last
349 two blocks was computed. The observer was excluded from further participation if their mean threshold
350 for the last two blocks in the practice session exceeded 0.025 ($\log T^2$, -3.2). This exclusion criterion was
351 specified in our preregistered protocol (See Methods: Preregistration).
352

353 Observers who met the performance criterion participated in the rest of the experiment.

354

355 Observer Information

356

357 A total of 17 observers participated in the practice sessions for the control and main experiments
358 (preregistered Experiments 2 and 3). To de-identify observer information in the data, observers were
359 numbered in the order they performed the practice sessions. 10 observers participated in the practice
360 sessions for the main experiment (preregistered Experiment 3; 6 Female, 4 Male; age 18-56; mean age
361 30.7). Four of these observers (Observer 2, Observer 4, Observer 8, and Observer 17) met the
362 performance criterion set for screening (2 Female, 2 Male; age 23-56; mean age 38.25). All observers
363 who advanced to the practice session had normal or corrected-to-normal vision (20/40 or better in both
364 eyes, assessed using Snellen chart) and normal color vision (0 Ishihara plates read incorrectly). The visual
365 acuities of the observers in the main experiment were: Observer 2, L = 20/30, R = 20/30; Observer 4, L =
366 20/15, R = 20/20; Observer 8, L = 20/30, R = 20/25; Observer 17, L = 20/20, R = 20/20. Observers 2, 8,
367 and 17 wore personal corrective eyewear both during vision testing and during the experiments. Observer
368 4 did not require or use corrective eyewear.

369

370 Apparatus

371 The stimuli were presented on a calibrated LCD color monitor (27-in. NEC MultiSync PA271W; NEC
372 Display Solutions) in an otherwise dark room. The monitor was driven at a pixel resolution of 1920 x
373 1080, a refresh rate of 60Hz, and with 8-bit resolution for each RGB channel. The host computer was an
374 Apple Macintosh with an Intel Core i7 processor. The experimental programs were written in MATLAB
375 (MathWorks; Natick, MA) and relied on routines from the Psychophysics Toolbox
376 (<http://psychtoolbox.org>) and mgl (<http://justingardner.net/doku.php/mgl/overview>). Responses were
377 collected using a Logitech F310 gamepad controller.

378 The observer's head position was stabilized using a chin cup and forehead rest (Headspot, UHCOTech,
379 Houston, TX). The observer's eyes were centered horizontally and vertically with respect to the display.
380 The distance from observer's eyes to the monitor was 75cm.

381 Monitor Calibration

382 The monitor was calibrated using a spectroradiometer (PhotoResearch PR650). To calibrate the monitor,
383 we focused the spectroradiometer on a patch displayed on the center of the monitor. The patch size was
384 4.66cm x 4.66cm (3.56° x 3.56°). The optics of the radiometer sampled the emitted light from a 1°
385 circular spot within the patch. The spectral power distribution of the three monitor primaries was
386 measured in the range 380nm to 780nm at 4nm steps. The gamma functions for each primary were
387 determined from measurements of the spectral power distribution for each primary at 26 equally spaced
388 input values for that primary, in the range [0, 1] where 1 corresponds to the maximum input value of the
389 device. These gamma functions as well as the light emitted by the monitor for an input of 0 were
390 accounted for in the stimulus display procedures. The spectral power distribution was also measured for
391 32 different combinations of RGB input values. These measurements were used to check the performance
392 of the display. The maximum absolute deviation of the x-y chromaticity between the measured values and
393 those predicted from the calibration was 0.0028 and 0.0027 for x and y chromaticity respectively, and less
394 than 1% for luminance.

395 Stimulus Presentation

396

397 The size of each image was 2.6cm x 2.6cm on the monitor, corresponding to 2° by 2° visual angle. The
398 target object size on the screen in the 2D images was ~1° in diameter. Each image was presented for

399 250ms (this was a deviation from the preregistration document, which specifies the presentation time as
400 500ms), with an inter-stimulus interval of 250ms and inter-trial interval of 250ms. Inter-stimulus interval
401 (ISI) is defined as the interval between the first and the second image presented on each trial. The
402 response for each trial was collected after both the images had been displayed and removed from the
403 screen. The observer could take as long as they wished before entering the response. Feedback was
404 provided via tones presented after the response to allow observers to maximize their performance. The
405 next trial was presented 250ms (ITI) after the feedback. Thus, the actual inter-trial interval depended on
406 the response time of the observer.
407

408 **Psychometric Function**

409 The proportion comparison chosen data was used to obtain the psychometric function for each block.
410 Each block consisted of 330 trials with 30 trials at each comparison lightness level. At each lightness
411 level, we recorded the number of times the observers chose the comparison image to be lighter. The
412 proportion comparison chosen data were fit with a cumulative normal using the Palamedes toolbox (Prins
413 & Kingdom, 2018) to obtain four parameters of the psychometric function: threshold, slope, lapse rate
414 and guess rate. The lapse rate was constrained to be equal to the guess rate and to be in the range [0,
415 0.05]. The psychometric function was fit using the maximum likelihood method. The threshold was
416 obtained as the difference between the LRFs at proportion comparison chosen 0.76 and 0.50 as obtained
417 from the cumulative normal fit.

418 **Ethics Statement**

419 All experimental procedures were approved by University of Pennsylvania Institutional Review Board
420 and were in accordance with the World Medical Association Declaration of Helsinki.

421 **Code and Data Availability**

422 For each observer, the proportion comparison chosen data for the 18 experimental blocks as well as the
423 thresholds are provided as supplementary information (SI). The SI also provides the MATLAB scripts to
424 generate Figures 2, 4, 5, 6 and 7 and the scripts to obtain thresholds of the linear receptive field
425 formulation of the model (model described below). The computed retinal images used as input to the
426 model are provided as .mat files in a zip folder. The SI is available at:
427 <https://github.com/vijaysoophie/EquivalentNoisePaper>.

428 **3 MODEL**

429 The data collected in the experiments characterize how lightness discrimination thresholds increase with
430 the variance of a task-irrelevant stimulus variable. Interpreting the data is aided by a model that relates the
431 changes in discrimination thresholds to the underlying precision of the perceptual representation. The
432 model provides a way to connect the variance of a task-irrelevant property to the precision of the
433 perceptual representation of the task-relevant stimulus variable (here lightness). The model we employ
434 shares features of models that have been used to understand how contrast thresholds are elevated in the
435 presence of contrast noise (see e.g., Legge, Kersten, & Burgess, 1987; Pelli, 1990). We provide a full
436 development of the model here, however, as the current application of the underlying ideas differs
437 substantially from previous applications.

438 We first introduce an analytic formulation, derived in the context of signal detection theory (SDT)
439 formulation). We then show how this can be instantiated as a linear receptive field model whose

440 performance can be simulated (LINRF formulation). An important advantage of the LINRF formulation is
441 that it can accommodate the physical-realizability constraint incorporated into our statistical model of
442 naturally occurring reflectances.

443 The model allows us to express the variation of the task-irrelevant stimulus variable in units of equivalent
444 noise standard deviation, where an equivalent noise standard deviation of 1.0 corresponds to the amount
445 of external variation whose effect on the perceptual representation of the task-relevant stimulus variable is
446 the same as that of the intrinsic internal noise that limits discrimination in the absence of task-irrelevant
447 external variation. In this way, we can understand the effect of the task-irrelevant variability on thresholds
448 in perceptually meaningful units of equivalent noise level. Task-irrelevant variability with an equivalent
449 noise level less than one have little impact on the visual system, since its effects are dominated by
450 intrinsic variability. Levels of task-irrelevant variability with an equivalent noise level greater than one do
451 intrude on perception. The equivalent noise level indicates the magnitude of the intrusion in units that
452 connect to intrinsic precision. Equivalent noise is similarly used in the literature on contrast noise
453 masking (again see e.g., Legge, Kersten, & Burgess, 1987; Pelli, 1990).

454 **SDT Model Formulation**

455 We first formulate our model in the context of signal detection theory (Green, 1966). We model the visual
456 response to the target object in each image by a univariate internal representation denoted by the variable
457 z . This variable depends on the image and is perturbed by noise. We assume that for any fixed image, z is
458 a normally-distributed random variable whose mean depends on the target object LRF. For each image,
459 we assume that z is perturbed on a trial-by-trial basis by independent zero-mean normally-distributed
460 noise, and we assume that the variance of this noise is the same for the response to all images. We refer to
461 the noise that perturbs z for a fixed image as the internal noise and denote its variance as σ_i^2 . For each
462 trial of the experiment, z takes on two values, z_s and z_c , one for the interval containing the standard and
463 the other for the interval containing the comparison.

464 If we consider performance for a particular pair of target standard and comparison LRFs, performance
465 depends both on the difference between the expected values of z for each pair of LRFs, μ_s and μ_c , and on
466 the value of σ_i^2 . In our experimental design we have ensembles of images with different backgrounds, for
467 each value of the target object LRF and background covariance scalar. The fact that we draw
468 stochastically from these ensembles on each trial introduces additional variability into the value of the
469 decision variable z that corresponds to a fixed target LRF. We call this the external variability, and model
470 it as a normal random variable with zero mean and variance σ_e^2 . We assume that σ_e^2 depends on the
471 experimentally chosen covariance scalar, but not on the target sphere LRF. Thus, the distributions of z_s
472 and z_c , for a particular choice of target standard and comparison LRF and covariance scalar, are given by
473 $P(z_s) = N(\mu_s, \sigma_t)$ and $P(z_c) = N(\mu_c, \sigma_t)$. Here μ_s is the mean value of the internal representation to the
474 standard image and μ_c is the mean value of the internal representation to the comparison image. The
475 overall standard deviation σ_t is obtained via $\sigma_t^2 = \sigma_i^2 + \sigma_e^2$, where σ_i^2 and σ_e^2 are the variance of the
476 internal and external noise.

477 For a 2AFC discrimination task in the context of signal detection theory, the observer makes their
478 decision based on a comparison of z_s and z_c , choosing the interval with the higher value of z as that with
479 the higher stimulus value. The observer's sensitivity depends on the mean values and the variance of z ,
480 and is captured by the quantity d-prime: $d' = (\mu_c - \mu_s)/\sigma_t$. D-prime measures the distance between the
481 two distributions in standard deviation units. A value of $d' = 0$ corresponds to an inability to distinguish
482 between the standard and the comparison image. Larger values of d' indicate increasing discriminability.

483 For a fixed value of d' , the difference in mean values is directly proportional to the standard deviation σ_t :

484 $(\mu_c - \mu_s) = d' \sigma_t = d' \sqrt{(\sigma_i^2 + \sigma_e^2)} .$ (1)

485 We further assume that the difference in mean value of the internal variable ($\mu_c - \mu_s$) is proportional to
 486 the difference in the LRFs of the target object in the standard and comparison images (Δ_{LRF}). That is,
 487 $(\mu_c - \mu_s) = C \Delta_{\text{LRF}}$, where C is the proportionality constant. This yields
 488

489 $\Delta_{\text{LRF}} = \frac{d'}{C} \sqrt{(\sigma_i^2 + \sigma_e^2)} .$ (2)

490 When we measure threshold in a 2AFC task, we choose a criterion proportional correct and find the Δ_{LRF}
 491 that corresponds to that proportion correct. Our choice of 0.76 corresponds to $d' = 1$. In addition we can
 492 choose $C = 1$, in essence setting the units for z to match those of the target LRF.

493 In our experiment, external variability was induced by changing the reflectance of the objects in the
 494 background. We used a multivariate normal distribution to generate the reflectance functions of the
 495 background objects.⁵ To change the amount of external noise, we scaled the covariance of the
 496 multivariate normal distribution by multiplying its covariance matrix with a scalar. Thus, for our
 497 experiments we have

498 $\Delta_{\text{LRF}} = \sqrt{\sigma_i^2 + \sigma^2 \times \sigma_{e0}^2}$ (3)

499 where σ^2 is the covariance scalar and σ_{e0}^2 is the external noise introduced when the ensemble of images
 500 for each value of target LRF has the reflectance of the background objects drawn from our model of
 501 natural reflectances.

502
 503 Converting the equation above to the form we use to represent the data, we have

504 $\log(\Delta_{\text{LRF}}^2) = \log(\sigma_i^2 + \sigma^2 \times \sigma_{e0}^2) .$ (4)

505 The equation above predicts that the form of threshold $\log(\Delta_{\text{LRF}}^2)$ as a function of covariance scalar σ^2
 506 should increase monotonically. For small values of σ^2 ($\sigma^2 \ll \sigma_i^2/\sigma_{e0}^2$), the threshold will approach a
 507 constant giving $\log(\Delta_{\text{LRF}}^2) \sim \log(\sigma_i^2)$. For large values of σ^2 ($\sigma^2 \gg \sigma_i^2/\sigma_{e0}^2$), the quantity $\log(\Delta_{\text{LRF}}^2)$ will
 508 approach a straight line with slope 1 in the $\log(\Delta_{\text{LRF}}^2)$ versus $\log(\sigma^2)$ plot. Fitting the measurements with
 509 Equation 4 allows us to check whether the model describes the data, as well as to determine the two
 510 parameters σ_i^2 and σ_{e0}^2 . In particular, we can establish the relative contribution of the internal
 511 representational variability and external stimulus variability in limiting lightness discrimination. The
 512 parameter σ_{e0}^2 quantifies how much the variation in background object reflectances intrudes on the
 513 internal representation z that mediates the lightness discrimination task. The value of σ_{e0}^2 may be
 514 compared directly to the intrinsic precision of that representation characterized by σ_i^2 .

515 **Equivalent Noise Level**

516 The SDT formulation allows us to introduce the concepts of equivalent noise and equivalent noise level.
 517 The equivalent noise is the amount of external variation that has the same effect on the decision variable z

⁵ Here we neglect the effect of the fact that we truncated the distribution to enforce a requirement that reflectance at each wavelength lies between 0 and 1. We return to account for this in the LINRF formulation below.

518 as the internal noise. The external variation is characterized experimentally by the covariance scalar
 519 (together with the underlying model of natural reflectances which is held fixed across the experiments).
 520 Once the model parameters σ_i^2 and σ_{e0}^2 are determined from the data, we can find the covariance scalar
 521 σ_{equiv}^2 that produces externally-generated equivalent noise

522
$$\sigma_{equiv}^2 = \sigma_i^2 / \sigma_{e0}^2. \quad (5)$$

523 This in turn allows us to express the covariance scalars in terms of their equivalent noise level, which
 524 gives their effect on the perceptual representation relative to the effect of the internal noise. Thus

525
$$\sigma_{enl}^2 = \sigma^2 / \sigma_{equiv}^2. \quad (6)$$

526 For $\sigma_{enl}^2 \ll 1$, the effect of the external noise is negligible and does not affect the perceptual
 527 representation and the internal noise dominates the precision of the representation. For $\sigma_{enl}^2 \gg 1$, the
 528 effect of the external noise dominates the perceptual representation, and the visual system has not
 529 insulated the representation of the task-relevant stimulus variable from the variation in the task-irrelevant
 530 perceptual variable. When the equivalent noise level is ~ 1 , the effect of the external variability is matched
 531 to that of the internal variability. At this operating point, further insulation of the task-relevant
 532 representation will not lead to significant further increases in the precision of this representation. We can
 533 thus use the equivalent noise level as a calibrated metric for assessing the magnitude of the perceptual
 534 effect of various levels of task-irrelevant stimulus variation.

535 Linear Receptive Field Formulation

536 When external noise added to the images is characterized by a multivariate normal and the decision noise
 537 is normal, a simple linear receptive field (LINRF) formulation is equivalent to the SDT formulation
 538 developed above. We develop this equivalence below. The advantage of the LINRF formulation is that it
 539 can easily be applied directly to images and to cases where the internal or external variability is non-
 540 normal. In our application, there are two non normalities. First, although the projection weights for linear
 541 model of naturally-occurring reflectance are drawn from a multivariate normal distribution, the constraint
 542 that the resulting reflectance functions lie within the range between 0 and 1, implemented to satisfy
 543 physical realizability, makes the overall distribution non-normal. Second, we incorporate into the model
 544 the Poisson variability of the cone excitations.

545 We begin with development that connects the LINRF formulation to the SDT formulation. In the LINRF
 546 formulation, the decision variable is computed from the displayed stimulus as the response of a single unit
 547 whose responses are a linear function of the stimulus image. Denote the stimulus image by the column
 548 vector I , and the receptive field by the column vector R . The entries of I are the radiant power emitted by
 549 the monitor at each image location. The entries of R are the corresponding sensitivities of the linear
 550 receptive field to each entry of I . The response of the receptive field is given as $r_i = R^T I + \eta_i$, where η_i
 551 is a random variable representing a draw of zero mean normally-distributed internal noise (variance σ_{ri}^2)
 552 in the receptive field response for a fixed image. We assume that σ_{ri}^2 is independent of I .

553 Denote I_{s0} and I_{c0} as the standard and comparison images without external noise. External normally-
 554 distributed noise is added to both I_{s0} and I_{c0} , with covariance matrix Σ_e . The external noise need not have
 555 zero mean. After incorporation of the external noise, the response of the receptive field to the comparison
 556 and standard images is given by

557
$$r_{ic} = R^T (I_{c0} + \eta_e) + \eta_i = R^T I_{c0} + \eta \quad (7)$$

$$558 \quad r_{is} = R^T(I_{so} + \eta_e) + \eta_i = R^T I_{so} + \eta. \quad (8)$$

559 Here η_e is a random variable representing a draw of external noise, η_i represents the internal noise, and η
 560 is a random variable representing the overall effect of the external and internal noise. Since the receptive
 561 field and noise models are linear and normal, η is normal with variance

$$562 \quad \sigma_{\eta}^2 = (\sigma_{ri}^2 + R^T \Sigma_e R). \quad (9)$$

The mean difference between the receptive field response to the comparison and the standard image is given by $(\mu_c - \mu_s) = R^T(I_{c0} - I_{s0}) = C'\Delta_{LRF}$. Here I_{s0} and I_{c0} are the standard and comparison images without external noise added, C' is a constant, and Δ_{LRF} is as defined in the SDT section above. The second equality follows because 1) the difference between I_{c0} and I_{s0} is proportional to Δ_{LRF} as only the target LRF changes between these two images and 2) even if the mean of the external noise is non-zero, its effect cancels when we obtain the mean difference in response.

569 We associate the linear receptive field response with the internal representation z of the SDT formulation
 570 developed above. That is, we assume that on each trial, the observer chooses as lighter the interval for
 571 which the response of the receptive field is greater. Following the development of the SDT formulation,
 572 we have

$$573 \quad \Delta_{\text{LRF}} = \frac{d'}{C'} \sqrt{\sigma_{ri}^2 + \sigma^2 \times (R^T \Sigma_{e0} R)} \quad (10)$$

where we have introduced the covariance scalar σ^2 in the term corresponding to the variance of the external noise, and where Σ_{e0} denotes the covariance matrix of the external noise corresponding to the level of variation in natural images. Comparing to relation derived in the SDT model (Equation 3), we see that this is the same functional form for the relation between Δ_{LRF} and σ^2 as derived there, where we associate $\sigma_i^2 = \frac{\sigma_{ri}^2}{(C')^2}$ and $\sigma_{e0}^2 = \frac{(R^T \Sigma_{e0} R)}{(C')^2}$.

To fit the LINRF formulation and relax its assumptions, we compute how images produce retinal cone excitations and employ a one-parameter description of a simple center-surround receptive field that draws upon the output of the cones. We use simulation to compute model responses for any choice of σ_i^2 . This procedure is described in more detail below. Once the fitting procedure establishes R and σ_i^2 that best account for the data, we then find σ_{e0}^2 directly by passing the images corresponding to $\sigma^2 = 1$ through the receptive field and finding the resulting variance. These parameters in turn allow us to compute σ_{equiv}^2 and σ_{enl}^2 for the LINRF formulation.

586 Fitting the SDT Model Formulation

The model was fit to the threshold versus covariance scalar data to obtain the parameters σ_i^2 and σ_e^2 . The parameters were obtained by minimizing the mean squared error between the measured and predicted threshold using the MATLAB function *fmincon*. The best fitting parameters were estimated separately for the mean observer and the individual observers.

591 Fitting the Linear Receptive Field Model Formulation

592 We fit the linear receptive field (LINRF) model using a simulation approach. We used simulation for two
 593 reasons. First, it allows us to incorporate a model of the early visual system into the computations.

594 Second, it provides a way to account for truncation in the normally-distributed model of natural
595 reflectances.

596 The model of initial visual encoding was as described by Singh et al. (2018), and was implemented using
597 the software infrastructure provided by ISETBio (ISETBio; isetbio.org; Cottaris, Jiang, Ding, Wandell, &
598 Brainard, 2019). It incorporated typical optical blur (Thibos, Hong, Bradley, & Cheng, 2002) and the
599 Poisson noise that perturbs cone photoreceptor isomerizations in the retina (Rodieck, 1998). In addition, it
600 included axial chromatic aberration (Marimont & Wandell, 1994), and spatial sampling by the mosaic of
601 long (L), middle (M) and short (S) wavelength-sensitive cones (Brainard, 2015). The L:M:S cone ratio in
602 the cone mosaic was chosen to be 0.6:0.3:0.1 (1523 L-cones, 801 M-cones, 277 S-cones). The CIE
603 physiological standard (CIE, 2007), as implemented in ISETBio, was used to obtain LMS cone
604 fundamentals. Cone excitations were calculated as the number of photopigment isomerizations in a 100ms
605 integration time, and included simulation of the Poisson variability of the isomerizations (Rodieck, 1998).
606 The cone isomerizations were demosaiced using linear interpolation to estimate LMS isomerization
607 images. Further, the isomerizations of each cone class was normalized by the summed (over wavelength)
608 quantal efficiency of the corresponding cone class, to make the magnitude of the signals from the three
609 cone classes similar to each other. This normalization occurred after incorporation of Poisson noise and
610 did not affect the signal-to-noise ratio of the signals from the different cone classes.

611 The dot product of the LMS isomerization images was taken with a simple center-surround linear
612 receptive field. The receptive field was square in shape to match the image size. Its center was a circle of
613 radius equal to the size and at the location of the target object in the image. The central region was taken
614 to have spatially-uniform positive sensitivity, while the surround was taken to have spatially-uniform
615 negative sensitivity. Each point in the central region had sensitivity $v_c = 1$, and each region of the
616 surround had sensitivity denoted by v_s . The RF was the same for each of the three cone classes. The RF
617 response was taken as the sum of the L, M and S RF component responses. Normally-distributed internal
618 noise with zero mean was added to the resulting dot product. The variance of the internal noise (σ_{ri}) and
619 the value of the RF surround sensitivity (v_s) were the two parameters of the model.

620 The threshold predictions of the LINRF formulation for any choice of model parameters were obtained
621 using simulation of a two-interval forced choice paradigm similar to the experiment. For each trial, we
622 randomly sampled a standard image and a comparison image from our dataset, following the procedure
623 used in the experiment. We obtained the response of the receptive field (noise-added dot product) to the
624 images and compared them to determine the simulated choice on that trial. This process was repeated
625 10,000 times for each of the 11 comparison LRF levels. The proportion comparison chosen data were
626 used to fit the psychometric function and obtain the discrimination threshold, similar to the method used
627 for the human psychophysical data. We estimated model threshold for the six values of covariance scalar
628 at which we performed the human experiments.

629 We calculated the mean squared error (averaged over the six covariance scalar values) between the
630 thresholds of the human data being fit and the computational model for a large set of values of the two
631 model parameters: the variance of the decision noise (σ_{ri}) and the value of the RF surround (v_s). The
632 mean squared error values obtained as a function of these two parameters were fit with a degree two
633 polynomial of two variables using the MATLAB *fit* function. The resulting polynomial was evaluated to
634 estimate the parameters with lowest mean square error. These parameters were then used to estimate the
635 internal and external noise standard deviation of the LINRF formulation using the relations: $\sigma_i^2 = \frac{\sigma_{ri}^2}{(C')^2}$
636 and $\sigma_{e0}^2 = \frac{(R^T \Sigma_{e0} R)}{(C')^2}$ as explained above, where the constant C' was obtained by solving $R^T(I_{c0} - I_{s0}) =$
637 $C' \Delta_{\text{LRF}}$.

638 The best fitting parameters were estimated separately for the mean observer and the individual observers.

639 **4 RESULTS**

640

641 **Human Lightness Discrimination Thresholds Increase with Background Reflectance Variation**

642

643 We measured lightness discrimination thresholds of human observers as a function of the amount of
644 variation in the reflectance spectra of the background objects in the scene. The amount of variation was
645 determined by the covariance matrix of the multivariate normal distribution from which the spectra were
646 sampled. We controlled the variance by multiplying the covariance matrix by a covariance scalar (σ^2).
647 We measured discrimination thresholds of four human observers at six values of the covariance scalar.
648 The threshold was measured three times (three separate blocks) for each observer and for each value of
649 covariance scalar. The psychometric functions for each block/covariance scalar value are shown for one
650 observer in Figure 4 and for all observers in Figure S3. Inspection of the psychometric functions shows
651 that their slopes steadily decrease with increasing covariance scalar, corresponding to an increase in
652 thresholds.

653

654 Figures 5 and 6 show the data in more digested form. These plots show explicitly how the discrimination
655 thresholds change with the amount of variability in the reflectance of the background objects. In Figure 5,
656 mean log threshold squared (averaged across observers, $N = 4$) is plotted against the log of the covariance
657 scalar. Figure 6 plots thresholds in the same format for the individual observers, with the data averaged
658 over the three blocks for each covariance scalar. The choice to plot the data as log threshold-squared
659 against the log of the covariance scalar was motivated by the relatively simple expression of the SDT
660 model formulation's predictions for this representation (see Equation 4 and following text). Table S2
661 provides the thresholds and SEMs from Figure 6 in tabular form.

662

663 For low values of the covariance scalar, the thresholds are nearly constant and are similar across
664 observers. As the covariance scalar increases, log squared threshold rises. These features are seen in the
665 mean data (Figure 5) and in the data for all observers (Figure 6). The covariance scalar value at which
666 thresholds start to increase is also similar across observers. There is some individual variability, however,
667 in the slope of the rising limb of the measured functions.

668

669 **Modeling the Impact of Background Reflectance Variation**

670

671 To interpret the data further, we fit the data with two formulations of our model (see Model section
672 above). The performance of both the SDT and LINRF model formulations is determined by two
673 fundamental factors. The first factor is variability in the perceptual representation of lightness internal to
674 the visual system (i.e., internal noise, model parameter σ_i^2). The second factor is the effect of
675 experimentally-induced task-irrelevant stimulus variability (i.e., background object reflectance
676 variability) on the same perceptual representation (i.e. external noise, model parameter σ_{e0}^2). Roughly
677 speaking, threshold with no external variation (covariance scalar $\sigma^2 = 0$) establishes the level of the
678 internal noise, while the way threshold increases with covariance scalar determines σ_{e0}^2 . The fits
679 determine the parameters of the model as well as allow us to examine how well the model fits the data.

680

681 The fits to the mean observer data are shown in Figure 5; the fits to the individual observer data are
682 shown in Figure 6.

683

684 The fit of the analytic STD formulation (red curves) captures the main trends in the mean data and
685 similarly for the fits to the individual observer data. Detailed examination, however, reveals that this
686 formulation tends to overestimate thresholds in the low covariance scalar regime. An alternative way of

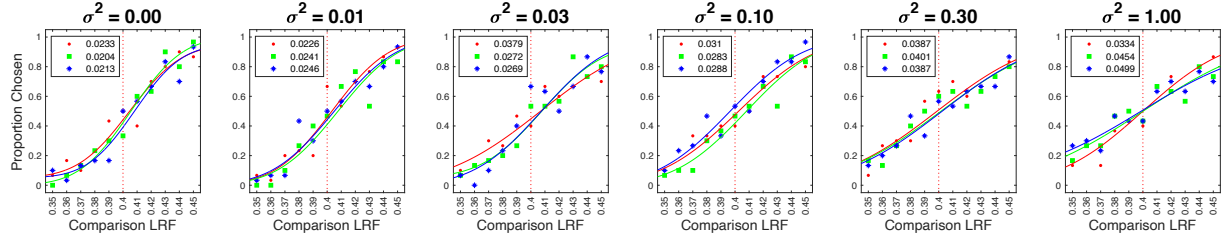


Figure 4: Psychometric functions for Observer 2. We measured the proportion comparison chosen data at six values of the covariance scalar (σ^2), separately in three blocks for each observer. The data for each block was fit with a cumulative normal to obtain the discrimination threshold (see Figure 2). Each panel plots the measured values and the cumulative fit to the proportion comparison data for each of the three blocks, for Observer 2. The values in the legend provide the estimate of lightness discrimination threshold for each block obtained from the cumulative fit. See Figure S3 for the psychometric functions of all observers.

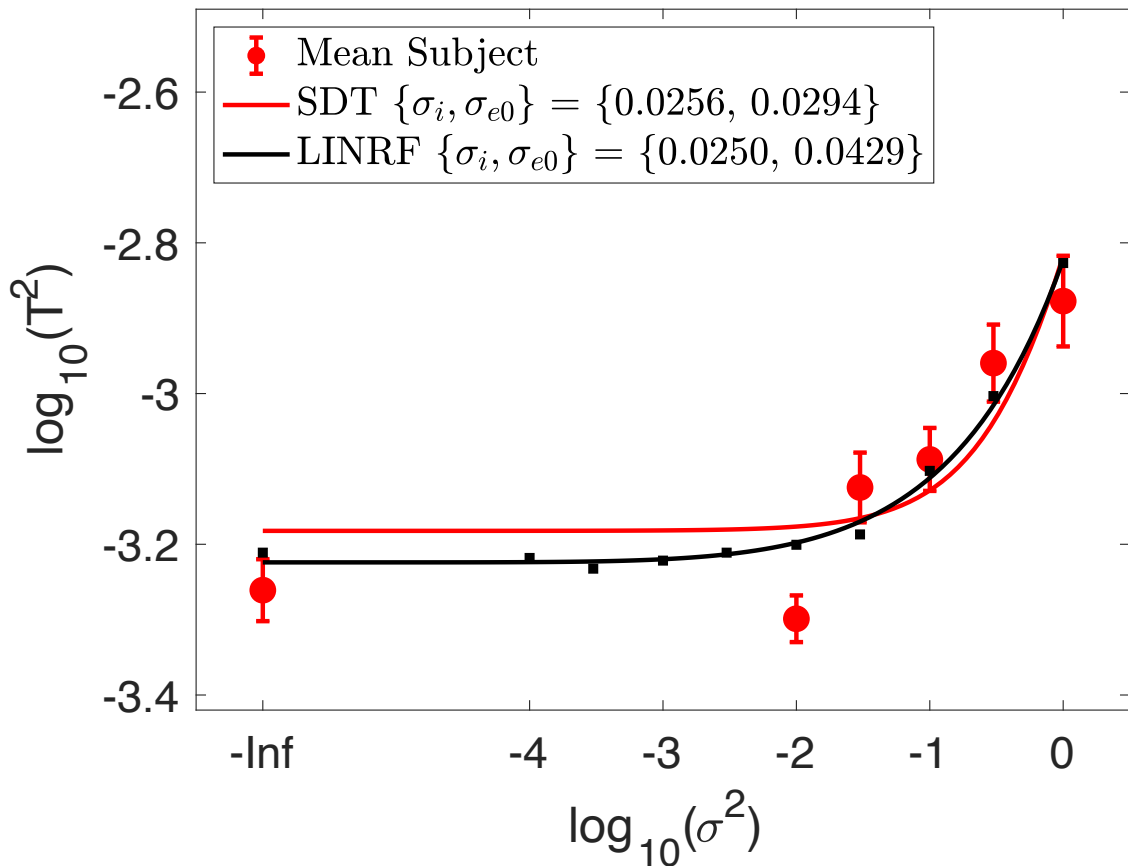


Figure 5: Background variation increases lightness discrimination threshold. Mean ($N = 4$) \log squared threshold vs \log covariance scalar from the human psychophysics (red circles). The error bars represent ± 1 SEM taken between observers. The fit of the STD formulation of the model (Equation 4) is shown as the red curve. The parameters corresponding to this fit are provided in the legend. The threshold of the fit linear receptive field (LINRF) formulation was estimated by simulation at 10 logarithmically spaced values of the covariance scalar (black squares). The black smooth curve is a smooth fit to these points of the functional form $\log_{10} T^2 = a + b^{(x+c)^d}$ where $x = \log_{10} \sigma^2$ and a, b, c and d are parameters adjusted in the fit. This functional form was chosen simply to provide a smooth curve through the simulated thresholds and has no theoretical significance. The parameters of the LINRF fit are also provided in the legend.

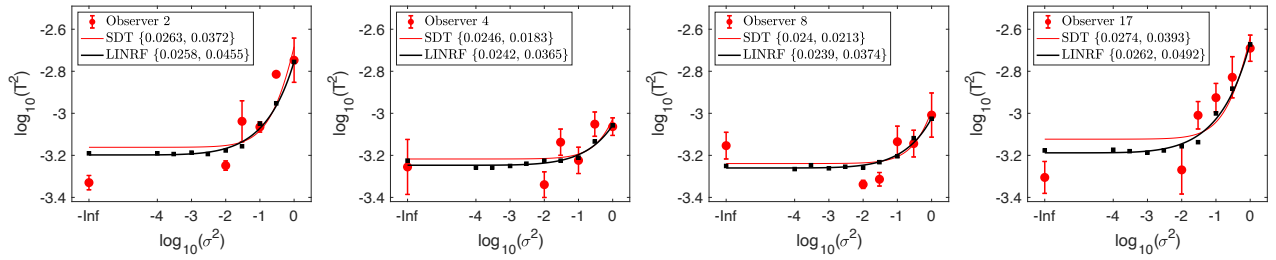


Figure 6: Threshold of individual human observers. Mean (across sessions) squared threshold vs log covariance scalar for individual human observers. Same format as Figure 5; here the error bars represent ± 1 SEM taken across the three blocks for each observer. The parameters of the SDT and LINRF formulations were obtained separately for each observer and are provided in the legend, in order $\sigma_i^2, \sigma_{e0}^2$.

687 putting this is that it underestimates the rising slopes as covariance scalar increases. Because the rising
688 slope of this formulation asymptotes to 1, the SDT formulation of the model is not able to simultaneously
689 describe thresholds over the full covariance scalar range.

690
691 The fits of the LINRF formulation (black curves) are better. The fit to the mean data does an excellent job
692 of capturing these data, and the fits to the individual observer data are also improved relative to the SDT
693 formulation. We attribute the improvement in fit of the LINRF formulation primarily to its ability to
694 account for the truncation of our experimental reflectance distributions, which the SDT formulation
695 cannot do (see Section 3 Model).

696
697 The model fits provide estimates of internal and external noise for the human observers in this task.
698 Figure 7 (left panel) plots the estimates of the internal and external noise standard deviations (quantities
699 σ_i and σ_{e0} , for both the SDT model and the LINRF formulation. There is good consistency in the value of
700 σ_i across observers, the model's manifestation of the observations that thresholds for low covariance
701 scalars are similar across observers. There is more variability in σ_{e0} across observers, corresponding to
702 the individual variability seen in the rising limb of the threshold versus covariance scalar plots.

703
704 The Poisson noise included in the LINRF formulation does not typically limit human discrimination
705 performance at daylight light levels (Banks, Geisler, & Bennett, 1987; Cottaris, Jiang, Ding, Wandell, &
706 Brainard, 2019). Thus, it is not surprising that the mean values of the internal noise standard deviation
707 parameter σ_i for the LINRF formulation are close to those obtained with the SDT formulation (SDT
708 formulation: mean value of internal noise standard deviation across observers 0.0256, value from fit to
709 mean data 0.0256; LINRF formulation: mean value of internal noise standard deviation across individual
710 observers 0.0250, value from fit to mean data, 0.0250).

711
712 The estimates of the external noise standard deviation parameter σ_{e0} are higher for the LINRF
713 formulation than for the SDT formulation (SDT formulation: mean value of external noise standard
714 deviation 0.0290, value from fit to mean data across observers 0.0294; LINRF formulation: mean value of
715 external noise standard deviation across observers 0.0421, value from fit to mean data, 0.0429). This is
716 consistent with the observation that the SDT formulation underestimates the rise in thresholds with
717 increasing covariance scalar, while this rise is captured more accurately by the LINRF formulation,
718 presumably because the latter incorporates the constraint that the reflectance values at each wavelength
719 are physically realizable (i.e., reflectances lie between 0 and 1).

720
721 If we focus on the estimates from the better fitting LINRF formulation, we can compute the equivalent
722 noise level (σ_{enl}) corresponding to covariance scalar $\sigma^2 = 1$, the level of background object reflectance
723 variation corresponding to our full model of natural reflectance. For the fits to the mean data, this
724 equivalent noise level is ~ 1.7 . This as well as values for the individual observers are plotted in the right
725 panel of Figure 7. This tells us that, for our experimental conditions, the variability in the human
726 representations of lightness induced by naturally occurring variation in background object reflectances is
727 within a factor of two of the limits imposed by the intrinsic precision of that representation. Had the value
728 been closer to 1, we would have concluded that the visual system had discounted the effect of variation in
729 the background object reflectances about as required, given the intrinsic precision of the lightness
730 representation. The fact the equivalent noise level is higher than 1 but not tremendously so is consistent
731 with the idea that the visual system has a degree of lightness constancy, but that this constancy can be
732 incomplete (see e.g., Gilchrist, 2006; Kingdom, 2011; Murray, 2021).

733
734 **5 DISCUSSION**

735
736 The perceived lightness of an object can depend on the scene in which it lies. Stabilization of the lightness
representation against variation in scene properties extrinsic to the object's surface reflectance is referred

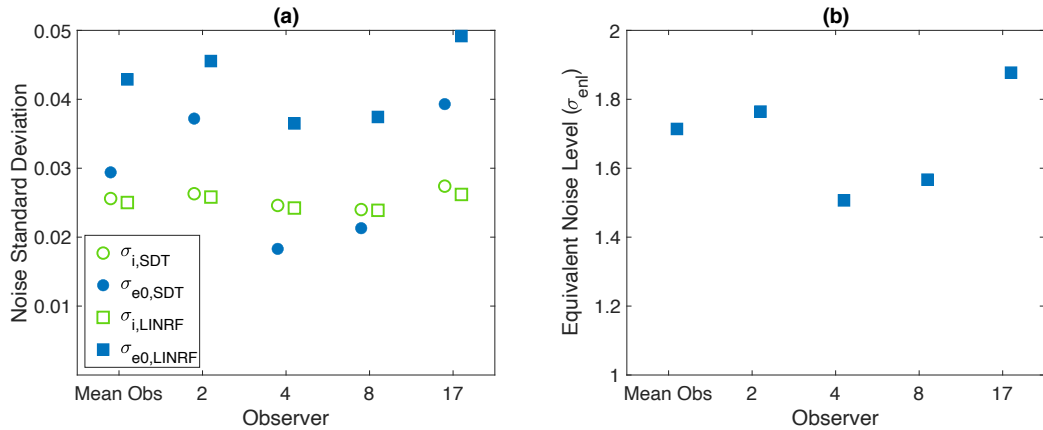


Figure 7. Equivalent noise analysis. **(a)** The left panel shows the parameter estimates for the two model formulations for the mean data and each individual observer. From these, we can estimate the equivalent noise level (σ_{enl}) for background object reflectance variation corresponding to the full model of natural reflectance variation (covariance scalar $\sigma^2 = 1$). **(b)** The equivalent noise level is provided for the mean data and each individual observer in the right panel.

to as lightness constancy. In this paper, we introduced a new psychophysical approach for characterizing lightness constancy. The approach is based on measuring how lightness discrimination thresholds vary with experimentally introduced variation in scene properties extrinsic to the object's reflectance. Specifically, we studied how lightness discrimination thresholds are impacted by variation in the reflectance of the background objects in naturalistic scenes rendered using computer graphics. Our results (Figures 5 and 6) show that when the variation in the reflectance of background objects is small, discrimination thresholds are nearly constant. In this regime, performance is limited primarily by internal noise. As the amount of background object reflectance variation increases, the effect of external variation starts dominating that of the internal noise, and discrimination thresholds increase. We analyzed the data using a modeling approach used previously to study effect of external noise on contrast detection (Legge, Kersten, & Burgess, 1987; Pelli, 1990; Pelli & Farell, 1999). This approach allows us to relate the effect of background object reflectance variation to the intrinsic precision of the lightness representation. The intrinsic precision depends on the observer's internal noise, which limits performance in the absence of external variation. The model compares discrimination thresholds with and without extrinsic variations to quantify variance in the perceptual representation of lightness induced by extrinsic variation. It allows us to express the effect of extrinsic variation as an equivalent noise level (σ_{enl}), that is relative to the standard deviation of the intrinsic noise. In this way, we use the intrinsic noise as a benchmark to interpret the magnitude of the equivalent noise from the external variation. We find that the effect of the external variability introduced by variation of background object reflectances in naturalistic scenes is within a factor of two of the intrinsic precision of the lightness representation. More generally, our work provides a method to quantify the effect of variation in a task-irrelevant properties on the perception of task-relevant property, and is thus applicable to understanding other perceptual constancies beyond the lightness constancy we focused on here.

Relation to Contrast Detection in Contrast Noise

As noted, our paradigm and model have conceptual roots in the literature on contrast detection in contrast noise. The concept of equivalent noise plays an important role in this literature (Legge, Kersten, & Burgess, 1987; Pelli, 1990 ; Pelli & Farell, 1999). However, there is an important difference between the way the ideas are applied to understand contrast detection and the way we have leveraged them here. In the contrast detection literature, detection in the absence of external noise is conceptualized as limited by two distinct factors. One factor is the internal variability in the observer's representation of contrast. The other factor is the efficiency with which the observer's decision processes makes use of the information provided by this representation, which is inferred through an ideal observer analysis applied to high external noise conditions, where effects of internal noise are swamped by those of the external noise (Pelli, 1990 ; Pelli & Farell, 1999). This separation is enabled when such an ideal observer calculation is available, and in practice is more straightforward when the stimulus being detected/discriminated and the external noise being added have commensurate units (e.g. contrast energy). In our work, the task-relevant and task-irrelevant stimulus variables vary along distinct dimensions of the stimulus space (e.g., affect distinct image locations). Currently we do not have in hand an ideal observer calculation that would allow us to compute the visual system's efficiency in using the available information. Obtaining and integrating such a calculation would be of interest. Singh, Cottaris, Heasly, Brainard, & Burge (2018) provide a possible approach, but employing that approach would require measurements with a larger set of task-irrelevant variation (e.g., illumination as well as background) than available from the current data.

Spatial and Chromatic Properties of the Stimuli

We used small image patches in our study. The small size of the image patches is a notable difference between our stimuli and natural viewing. In this initial deployment of our paradigm, we thus focused on effects of background object reflectance variation that are nearby the test object. The observed effects may be mediated by relatively small populations of neurons. The use of small image patches is not a

788 necessary requirement of our paradigm, which could be extended to larger images. Such extension could
789 reveal additional effects not captured by the current experiments.

790
791 In addition to using small patches, we did not vary the spatial structure of the array of objects in the
792 rendered scenes. Manipulating spatial structure, in addition to increasing image size, may provide a way
793 to use our paradigm to measure the spatial tuning of the mechanism(s) mediating the background effect.
794 This approach is loosely analogous to how manipulating the structure of contrast noise may be used to
795 examine the tuning of mechanisms supporting the detection of contrast-defined targets (Henning, Hertz,
796 & Hinton, 1981; Rovamo, Franssila, & Nasanen, 1992; Losada & Mullen, 1995; Nachmias, 1999;
797 Rovamo, Raninen, & Donner, 1999).

798
799 Although we restricted our measurements to lightness discrimination thresholds, our variation of the
800 reflectance properties of the background objects was not limited to variation in overall reflectance. The
801 choice to introduce background object reflectance variation along more spectral dimensions (affecting e.g.
802 background object hue and saturation) than used for target object variation was somewhat arbitrary – we
803 could have restricted the background object reflectance variation to one dimension (e.g. overall scale of
804 reflectance spectra) or studied discrimination of additional (e.g. chromatic) dimensions of target object
805 variation. As with the case of spatial structure above, extending the measurements to a wider range of
806 stimuli is of interest. Indeed, it may be possible to manipulate the chromatic structure of the variation in
807 background object reflectances with the goal of understanding the chromatic tuning of the background
808 object reflectance variation’s effect on the lightness discrimination thresholds, as well as on other target
809 object discriminations. This would again be analogous to how noise-based approaches have been used to
810 characterize chromatic tuning of mechanisms that support the detection of chromatically-defined contrast
811 targets (Gegenfurtner & Kiper, 1992; Sankeralli & Mullen, 1997; Julianini & Eskew, 1998; Monaci,
812 Menegaz, Süssstrunk, & Knoblauch, 2004).

813

814 **Link Between Thresholds and Suprathreshold Perceptual Judgments**

815

816 The technique developed here probes the constancy of a perceptual representation of a task-relevant
817 variable (e.g., perceived object lightness) by measuring how variation in a task-irrelevant scene variable
818 (e.g., background object reflectances) elevates thresholds for detecting changes in the task-relevant
819 variable. As with other threshold-based methods for approaching the stability of suprathreshold
820 perceptual judgments (see Introduction), the extent to which the results may be used to predict the
821 stability such judgments across changes in other scene variables is not known. Experiments that explore
822 this link, perhaps by directly comparing results from the two paradigms with similar stimuli and the same
823 set of observers, are of considerable interest. The results of such experiments might also be helpful in
824 pointing the way to theory that would link results across the two paradigms; at present we do not have
825 such theory in hand (but see Abrams, Hillis, & Brainard, 2007).

826
827 Previous authors have suggested that lightness constancy improves with increasing background
828 “articulation”. That is, increasing the number of objects in the background and/or the degree to which
829 their reflectance varies tends to improve constancy (Gilchrist, 2006; Radonjić & Gilchrist, 2013; see also
830 Radonjić, Cottaris, & Brainard, 2015; Kraft, Maloney, & Brainard, 2002). This may on the surface seem
831 in contradiction to our results; we find increasing the variance of the background reflectances has a
832 deleterious effect on lightness discrimination performance. Note, however, that articulation is thought to
833 improve constancy when the task-irrelevant variation is a change in illumination, and where the
834 background itself is held fixed across this change. In our experiments, the illumination is held fixed and
835 we consider the effect of the background per se, with the background change occurring across the two
836 intervals of each forced-choice trial. Thus, we are studying a different aspect of lightness constancy than
837 where increased articulation is thought to lead to improvements, and our results are not in conflict with
838 previous findings.

839
840 Our paradigm could be used to study constancy across changes in illumination, if the task-irrelevant
841 variation used in the experiment were in the illumination rather than the background object reflectances.
842 In that case, the articulation idea would predict a smaller elevation of lightness discrimination thresholds
843 when the effect of illumination variation was studied for scenes with higher variance in the background
844 reflectance, as long as the background was held fixed across the two intervals of each trial.
845

846 Applications to Understanding Neural Mechanisms

847

848 A longstanding goal of vision science is to connect psychophysical performance to its underlying neural
849 mechanisms. For probing mechanisms that mediate perceptual constancies, our paradigm has the
850 attractive feature that there is a well-defined correct answer on each trial, so that for studies with animal
851 subjects it is possible to provide performance-contingent reward. In addition, there are well-worked out
852 methods for predicting psychophysical discrimination performance from recordings of the responses of
853 neural populations (Shadlen, Britten, Newsome, & Movshon, 1996; Parker & Newsome, 1998; Cohen &
854 Newsome, 2009; Nienborg, Cohen, & Cumming, 2012; Ruff, Ni, & Cohen, 2018), and the theoretical
855 links between such analysis and performance should continue to hold when task-irrelevant stimulus
856 variation is added to the paradigm. Complementing neural measurements that include random,
857 unpredictable task-irrelevant stimulus variation with such analyses may provide rigorous quantitative
858 insights about the sensory-perceptual processing and the neural computations underlying color and
859 lightness constancy specifically, and perceptual constancy more generally.
860

861 Model of Natural Surface Reflectances

862

863 We used a truncated multivariate normal distribution as the statistical model for the projection weights of
864 a linear model of naturally occurring reflectances, to sample the background object reflectance functions.
865 This model was developed in our earlier work and is evaluated more fully there (Singh, Cottaris, Heasly,
866 Brainard, & Burge, 2018; see also Brainard & Freeman, 1997; Zhang & Brainard, 2004). The model is
867 based on measurements of the surface reflectance functions of the Munsell papers (Kelly, Gibson, &
868 Nickerson, 1943) as well as natural surfaces characterized by Vrhel (1994). The underlying multivariate
869 normal provides a convenient way to capture two basic aspects of natural variation in reflectance. First,
870 these reflectances are well-described by low-dimensional linear models (Cohen, 1964; Maloney, 1986;
871 Parkkinen, Hallikainen, & Jaaskelainen, 1989). Second, within the reflectance subspace defined by the
872 linear models, not all reflectances are equally likely to occur. Still, we think it likely that future work will
873 lead to more accurate statistical models of naturally occurring reflectance. For example, it is possible that
874 replacing the linear model approach with a prior that favors spectrally-smooth reflectance functions
875 (Jiang, Farrell, & Wandell, 2016) would lead to a more accurate characterization. In addition, we have
876 assumed that the distribution of reflectance functions over objects is independent, but this assumption
877 may not be accurate. Approaches to modeling a dependency have been suggested (Shen & Yeo, 2011;
878 Gehler, Rother, Kiefel, Zhang, & Schölkopf, 2011; Barron & Malik, 2012b; Barron & Malik, 2012a).
879

880 It is important to note that the quantitative relation we measured between the magnitude of internal noise
881 and the effect of external noise introduced as variation in background object reflectances depends on how
882 the distribution of naturally-occurring reflectances is modeled. If the model of reflectances overestimates
883 the natural variation, the effect of external noise in natural scenes will be less than we estimated.
884 Conversely, if the model of reflectances underestimates the natural variation, the effect of external noise
885 in natural scenes will be greater than we estimated. Importantly, improved future characterization of
886 naturally occurring reflectances, obtained through the acquisition of additional reflectance measurements
887 and advances in their statistical description, could be used in conjunction with the parameters of the
888 LINRF model formulation, without need for new data collection, to update the estimate of the effect of
889 naturally occurring background object reflectance variation on object lightness perception.

890

891 **Rule of Combination**

892

893 In the present work, we considered variation in only a single task-irrelevant variable. In natural scenes,
894 there are many task-irrelevant variables. In the case of judging object lightness, these include object-
895 extrinsic factors such as the scene illumination, the position and 3D orientation of the target object in the
896 scene, the viewpoint from which the object is viewed, and various object-intrinsic factors like its shape
897 and size. Variation in each of the factors could in principle elevate thresholds for discriminating object
898 lightness. Our paradigm allows characterization of the effect of these task-irrelevant variables and
899 quantifies that effect for each such variable in the same internal-noise referred units. One potentially
900 important future direction is to measure the combined effect of simultaneous variation of multiple task-
901 irrelevant variables, and to test hypotheses about rules of combination that predict the joint effects of such
902 simultaneous variation.

903

904 **6 ACKNOWLEDGEMENTS:** NSF BCS 2054900 (VS), NIH R01 EY10016 (DHB), NIH R01
905 EY028571 (JB).

906

907 APPENDIX

908 **Measurement of object lightness discrimination thresholds under variation in background object**
909 **reflectances**

910 The control experiment, preregistered as Experiment 2, provided preliminary data that helped shape the
911 design of the main experiment presented in the paper (which was Experiment 3 of the preregistration
912 documents). It aimed to determine whether variation in the reflectance of background objects had an
913 effect on human lightness discrimination thresholds. It established that human object lightness
914 discrimination thresholds increase if the reflectances of background objects vary, as compared to the case
915 when the discrimination is made against a constant background. It also studied the effect of inclusion or
916 not of secondary reflections in the rendering process and assessed the effect of implementing background
917 object reflectance variation across trials rather than across intervals.

918 The basic methods were the same as for preregistered Experiment 3. The practice session was conducted
919 with the images in Condition 1 described below. The observers were retained for the experiment if their
920 average threshold of the last two blocks during the practice session was lower than 0.030. This was a
921 deviation from the preregistered plan where we set the threshold criterion as 0.025. After collecting data
922 from 8 observers, we realized that the criterion was too strict. Only one observer had met the criterion.
923 After modifying the threshold criterion, we included two of the initially discontinued observers in our
924 experiment (Observer 5 and Observer 8). A total of 11 naïve observers participated in the practice
925 sessions. Four of these observers met the criteria for continuing the experiment. Two of these observers
926 also participated in the main experiment (Observer 4 and Observer 8). The visual acuities of these 4
927 observers were: Observer 4, L = 20/15, R = 20/20; Observer 5, L = 20/20, R = 20/40; Observer 8, L =
928 20/30, R = 20/25; Observer 11, L = 20/25, R = 20/30. Observers 5, 8, and 11 wore personal corrective
929 eyewear both during vision testing and during the experiments. Observer 4 did not require or use
930 corrective eyewear.

931 We measured lightness discrimination threshold of four naïve human observers using a two-interval
932 forced choice paradigm. The thresholds were measured for three specific types of background variation
933 (Figure S1). The reflectance spectra of the background objects were generated with the covariance scalar
934 set to 1. These three conditions were:

935 *Condition 1. Fixed background:* In this condition, the spectra of objects in the background were kept
936 fixed for all trials and for all intervals. We generated 11 images, one at each comparison LRF level.

937 *Condition 2. Between-trial background variation:* In this condition, the spectra of the objects in the
938 background were the same for the two intervals within a trial but varied from trial-to-trial.

939 *Condition 3. Within-trial background variation:* In this condition, the spectra of the objects in the
940 background varied between trials as well as between the two intervals of a trial. The background variation
941 corresponded to covariance scalar equal to 1.

942 In Conditions 2 and 3, the light reflected from the target object varied from image to image (even at the
943 same LRF level of the target object) because of secondary reflection of light coming from the background
944 objects was included in the rendering. We also measured the thresholds without secondary reflections for
945 these two conditions. We call these conditions Condition 2a and 3a.

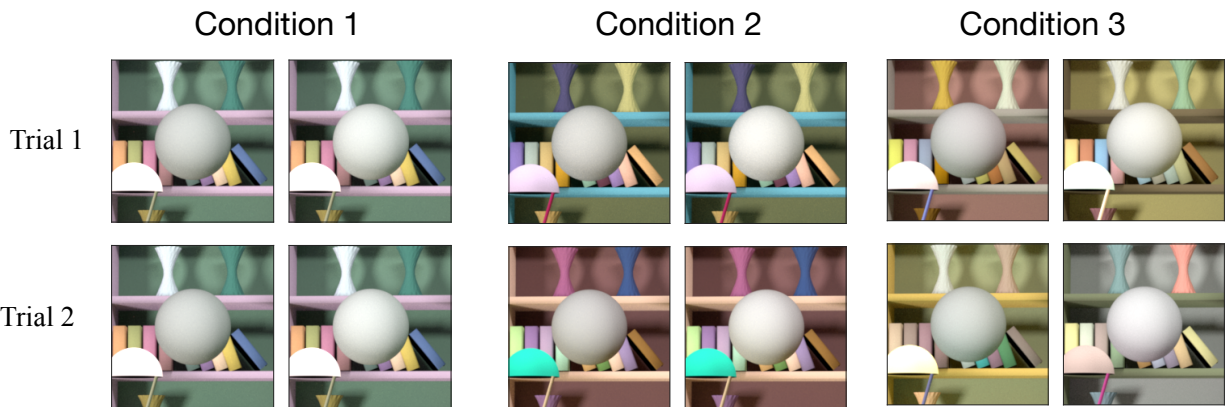


Figure S1: Control experiment stimuli. Example stimuli for Conditions 1, 2 and 3 in the control experiment (preregistered Experiment 2) to study the effect of variation in background object reflectances on lightness discrimination threshold. In condition 1, the background was fixed in every trial and every interval. In Condition 2, the background object reflectances varied from trial to trial, but remained fixed in the two intervals of a trial. In Condition 3, the background object reflectances varied in each trial and interval. For illustration, in this figure we have chosen the stimulus on the left to be the standard image with target object at 0.4 LRF and the on the right to be comparison image with target object at 0.45 LRF. In the experiment, the two images were presented sequentially in random order at the center of the screen. Conditions 2a and 3a stimuli are similar to Conditions 2 and 3 respectively, but without secondary reflections.

946 Condition 2a. Between-trial background variation without secondary reflection: Same as Condition 2, but
947 without multiple reflections of light from object surfaces. The light rays only bounce off once from the
948 surfaces before coming to the camera.

949 Condition 3a. Within-trial background variation without secondary reflections: Same as Condition 3, but
950 without multiple reflections of light from object surfaces. Condition 3a was the same as the experiment
951 reported in the main paper for covariance scalar equal to 1.

952 Figure S2 shows the discrimination thresholds of the four human observers for the five conditions studied
953 in this experiment. We plot the mean threshold and the standard error of the mean (SEM) taken over the
954 three separate threshold measurements. For each observer, the thresholds for Conditions 3 and 3a were
955 higher compared to Conditions 1, 2 and 2a. The average increases in threshold of the observers for
956 Conditions 3 and 3a as compared to Condition 1 (baseline) were 79% and 60% respectively. The average
957 increases in threshold for Conditions 2 and 2a were much smaller, 13% and 17% respectively. The
958 thresholds for Conditions 1, 2 and 2a were nearly within one SEM of each other (averaged over the
959 observers and three conditions). On the other hand, the thresholds for Conditions 3 and 3a were
960 respectively (on average) 7.2 and 5.4 SEM larger than the threshold of Condition 1. The thresholds
961 without secondary reflections (Conditions 2a and 3a) were within one SEM from the conditions with
962 secondary reflections (Conditions 2 and 3).

963 The control experiment established that lightness discrimination thresholds are higher for the case when
964 the two objects are being discriminated against different backgrounds on the same trial, as compared to
965 when the backgrounds are the same within trial. Trial-to-trial variability in background object reflectances
966 across trials has little, if any, effect. The effect is similar when the rendering is performed with and
967 without secondary reflections, indicating the effect is due to the spectral change in the background and
968 not due to the variation in the amount of light being reflected from the target object. In the main
969 experiment, we rendered without secondary reflections to avoid introducing such variability. Figure S2
970 also shows the threshold of the observers in the main experiment (preregistered Experiment 3) for the
971 condition with covariance scalar equal to 1. This condition is equivalent to Condition 3a of the control
972 experiment (preregistered Experiment 2). Thresholds were consistent across the two measurements.

973

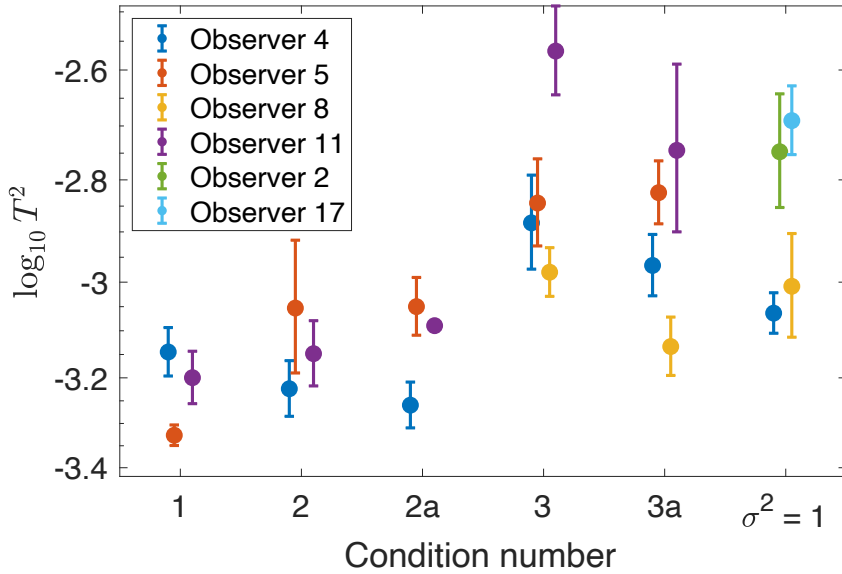


Figure S2: Control experiment. Lightness discrimination threshold of four human observers in the five conditions in the control experiment (preregistered Experiment 2). The plotted points have been jittered horizontally to avoid marker overlap. The thresholds are higher for the condition where the target objects are compared against a change in background object reflectances (Conditions 3 and 3a) than when the background is held fixed within each trial (Conditions 1, 2, 2a). Secondary reflections do not have any significant effect on thresholds (Conditions 2a and 3a). Condition 3a of the control experiment is equivalent to the condition of the main experiment (preregistered Experiment 3) with covariance scalar equal to 1. The thresholds for this condition of the main experiment are plotted here for comparison ($\sigma^2 = 1$). Two observers from the control experiment also participated in the main experiment.

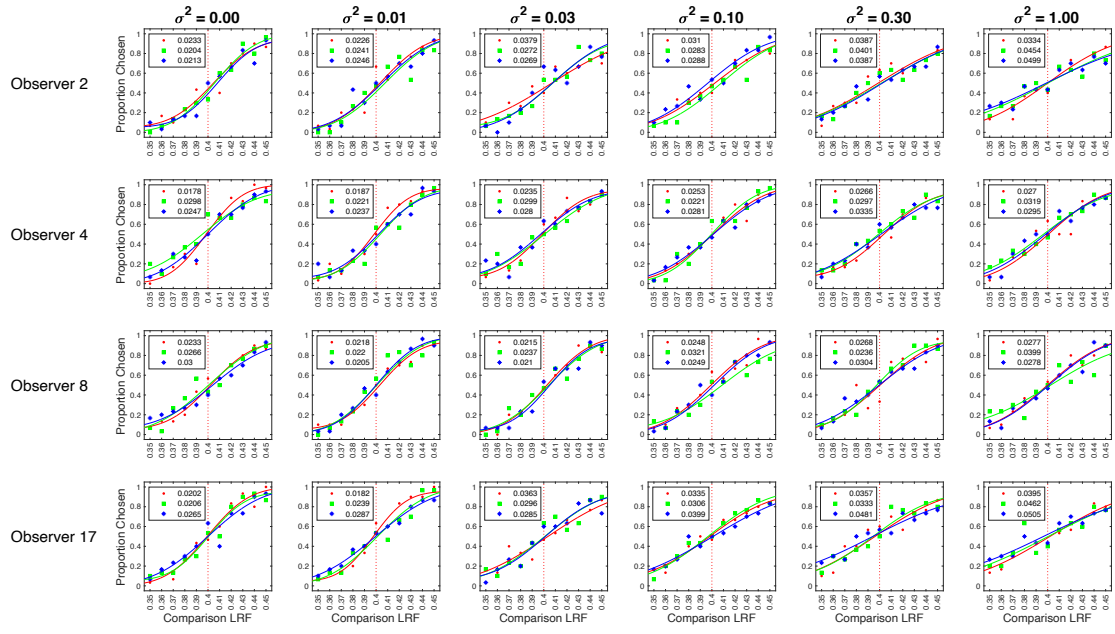


Figure S3: Psychometric functions for all observers. Same as Figure 4 for all observers retained in the main experiment.

974
975
976

Table S1: Thresholds for Control Experiment (Preregistered Experiment 2):
 Mean threshold (averaged over blocks) \pm SEM of four human observers for five background variation conditions studied in experiment 2.

Observer	Mean Threshold \pm SEM (averaged over sessions)				
	Condition 1	Condition 2	Condition 2a	Condition 3	Condition 3a
4	0.0269 \pm 0.0013	0.0254 \pm 0.0013	0.0235 \pm 0.0011	0.0366 \pm 0.0030	0.0330 \pm 0.0018
5	0.0217 \pm 0.0005	0.0305 \pm 0.0039	0.0300 \pm 0.0017	0.0382 \pm 0.0031	0.0389 \pm 0.0022
8	0.0167 \pm 0.0011	0.0169 \pm 0.0020	0.0175 \pm 0.0017	0.0325 \pm 0.0016	0.0273 \pm 0.0016
11	0.0252 \pm 0.0013	0.0268 \pm 0.0018	0.0285 \pm 0.0002	0.0525 \pm 0.0038	0.0439 \pm 0.0068

977
978
979
980
981
982

Table S2. Thresholds for Main Experiment (Preregistered Experiment 3):
 Mean threshold (averaged over blocks) \pm SEM of four human observers measured at six logarithmically spaced values of the covariance scalar.

Observer	Covariance Scalar					
	0	0.01	0.03	0.1	0.3	1
2	0.0217 \pm 0.0009	0.0238 \pm 0.0006	0.0307 \pm 0.0036	0.0294 \pm 0.0008	0.0392 \pm 0.0005	0.0429 \pm 0.0049
4	0.0241 \pm 0.0035	0.0215 \pm 0.0015	0.0271 \pm 0.0019	0.0246 \pm 0.0018	0.0299 \pm 0.0020	0.0295 \pm 0.0014
8	0.0266 \pm 0.0019	0.0214 \pm 0.0005	0.0221 \pm 0.0008	0.0273 \pm 0.0024	0.0269 \pm 0.0020	0.0318 \pm 0.0041
17	0.0224 \pm 0.0020	0.0236 \pm 0.0030	0.0315 \pm 0.0024	0.0347 \pm 0.0027	0.0390 \pm 0.0046	0.0454 \pm 0.0032

983
984

985 **Figure Captions**
986

987 **Figure 1: Psychophysical task.** **(a)** On every trial of the experiment, human observers viewed
988 two images in sequence, a standard image and a comparison image and indicated the one in
989 which the spherical target object in the center of the image was lighter. Example standard and
990 comparison images are shown. The images were computer graphics simulations. The simulated
991 reflectance functions of the target were spectrally flat, and the spheres appeared gray. The overall
992 reflectance of the target was held fixed in the standard images and differed between standard and
993 comparison. Performance (proportion correct) was measured as a function of this difference to
994 determine discrimination threshold. The reflectance spectra of objects in the background could
995 be held fixed or vary between standard and comparison on each trial (as illustrated here). The
996 order of presentation of the standard and comparison images was randomized from trial to trial.
997 Discrimination thresholds were measured as function of the amount of variation in background
998 object reflectances. **(b)** Trial sequence. R_{N-1} indicates the time of the observer's response for the
999 $(N-1)^{th}$ trial. The N^{th} trial begins 250ms after that response (Inter Trial Interval, ITI). The N^{th} trial
1000 consists of two 250ms stimulus presentation intervals with a 250ms inter-stimulus interval (ISI).
1001 The observer responds by pressing a button on a gamepad after the second stimulus has been
1002 shown. The observer can take as long as he or she wishes before making the response, with an
1003 example response time denoted by R_N in the figure. The next trial begins 250ms after the
1004 response.
1005

1006 **Figure 2: Psychometric function.** We recorded the proportion of times the observer chose the target in
1007 the comparison image to be lighter, as a function of the comparison LRF. The LRF of the target object in
1008 the standard image was fixed at 0.4. The LRF of the target object in the comparison image were chosen
1009 from 11 linearly spaced values in the range [0.35, 0.45]. In each block, thirty trials were presented at each
1010 comparison LRF value. We fit a cumulative normal distribution to the proportion comparison chosen data
1011 using maximum likelihood methods. The guess and lapse rates were constrained to be equal and were
1012 restricted to be in the range [0, 0.05]. The threshold was measured as the difference between the LRF at
1013 proportion comparison chosen equal to 0.76 and 0.5, as predicted by the cumulative normal fit. This
1014 figure shows the data for Observer 2 for scale factor 0.00, for the block run in the first experimental
1015 session for that observer. The point of subjective equality (PSE, the LRF corresponding to proportion
1016 chosen 0.5) was close to 0.4 as expected and the threshold was 0.0233. The lapse rate for this fit was 0.05.

1017 **Figure 3: Variation in background object reflectances:** The reflectance spectra of background objects
1018 were chosen from a multivariate normal distribution that modeled the statistics of natural reflectance
1019 spectra. The variation in the reflectance spectra was controlled by multiplying the covariance matrix of
1020 the distribution with a scalar. We generated images at six levels of the scalar. Each column shows three
1021 sample images at each of the six values of the scalar. The leftmost column corresponds to no variation
1022 and the rightmost column corresponds to the modeled variation of natural reflectances. The target object
1023 (sphere at the center of each panel) in each image has the same LRF. For each value of the scalar, we
1024 generated 1100 images, 100 each at 11 linearly spaced target LRF levels across the range [0.35, 0.45].
1025 Discrimination thresholds were measured separately for each value of the covariance scalar.
1026

1027 **Figure 4: Psychometric functions for Observer 2.** We measured the proportion comparison chosen data
1028 at six values of the covariance scalar (σ^2), separately in three blocks for each observer. The data for each
1029 block was fit with a cumulative normal to obtain the discrimination threshold (see Figure 2). Each panel
1030 plots the measured values and the cumulative fit to the proportion comparison data for each of the three
1031 blocks, for Observer 2. The values in the legend provide the estimate of lightness discrimination threshold

1032 for each block obtained from the cumulative fit. See Figure S3 for the psychometric functions of all
1033 observers.

1034

1035 **Figure 5: Background variation increases lightness discrimination threshold.** Mean ($N = 4$) log
1036 squared threshold vs log covariance scalar from the human psychophysics (red circles). The error bars
1037 represent ± 1 SEM taken between observers. The fit of the STD formulation of the model (Equation 4)
1038 is shown as the red curve. The parameters corresponding to this fit are provided in the legend. The
1039 threshold of the fit linear receptive field (LINRF) formulation was estimated by simulation at 10
1040 logarithmically spaced values of the covariance scalar (black squares). The black smooth curve is a
1041 smooth fit to these points of the functional form $\log_{10} T^2 = a + b^{(x+c)^d}$ where $x = \log_{10} \sigma^2$ and a, b, c
1042 and d are parameters adjusted in the fit. This functional form was chosen simply to provide a smooth
1043 curve through the simulated thresholds and has no theoretical significance. The parameters of the LINRF
1044 fit are also provided in the legend.

1045

1046 **Figure 6: Threshold of individual human observers.** Mean (across sessions) squared threshold vs log
1047 covariance scalar for individual human observers. Same format as Figure 5; here the error bars represent
1048 ± 1 SEM taken across the three blocks for each observer. The parameters of the SDT and LINRF
formulations were obtained separately for each observer and are provided in the legend, in order $\sigma_i^2, \sigma_{e0}^2$.

1049

1050 **Figure 7. Equivalent noise analysis.** (a) The left panel shows the parameter estimates for the two model
1051 formulations for the mean data and each individual observer. From these, we can estimate the equivalent
1052 noise level (σ_{eni}) for background object reflectance variation corresponding to the full model of natural
1053 reflectance variation (covariance scalar $\sigma^2 = 1$). (b) The equivalent noise level is provided for the mean
data and each individual observer in the right panel.

1054

1055 **Figure S1: Control experiment stimuli.** Example stimuli for Conditions 1, 2 and 3 in the control
1056 experiment (preregistered Experiment 2) to study the effect of variation in background object reflectances
1057 on lightness discrimination threshold. In condition 1, the background was fixed in every trial and every
1058 interval. In Condition 2, the background object reflectances varied from trial to trial, but remained fixed
1059 in the two intervals of a trial. In Condition 3, the background object reflectances varied in each trial and
1060 interval. For illustration, in this figure we have chosen the stimulus on the left to be the standard image
1061 with target object at 0.4 LRF and the on the right to be comparison image with target object at 0.45 LRF.
1062 In the experiment, the two images were presented sequentially in random order at the center of the screen.
1063 Conditions 2a and 3a stimuli are similar to Conditions 2 and 3 respectively, but without secondary
1064 reflections.

1065

1066 **Figure S2: Control experiment.** Lightness discrimination threshold of four human observers in the five
1067 conditions in the control experiment (preregistered Experiment 2). The plotted points have been jittered
1068 horizontally to avoid marker overlap. The thresholds are higher for the condition where the target objects
1069 are compared against a change in background object reflectances (Conditions 3 and 3a) than when the
1070 background is held fixed within each trial (Conditions 1, 2, 2a). Secondary reflections do not have any
1071 significant effect on thresholds (Conditions 2a and 3a). Condition 3a of the control experiment is
1072 equivalent to the condition of the main experiment (preregistered Experiment 3) with covariance scalar
1073 equal to 1. The thresholds for this condition of the main experiment are plotted here for comparison
($\sigma^2 = 1$). Two observers from the control experiment also participated in the main experiment.

1074

1075 **Figure S3: Psychometric functions for all observers.** Same as Figure 4 for all observers retained in the
main experiment.

1076

1077 REFERENCES
1078

- 1079 Abrams, A. B., Hillis, J. M., & Brainard, D. H. (2007). The relation between color discrimination
1080 and color constancy: when is optimal adaptation task dependent? *Neural Computation*,
1081 19, 2610-2637.
- 1082 Adelson, E. H. (1993). Perceptual organization and the judgment of brightness. *Science*,
1083 262(December 24), 2042-2044.
- 1084 Adelson, E. H. (2000). Lightness perception and lightness illusions. In M. Gazzaniga (Ed.), *The*
1085 *New Cognitive Neurosciences, 2nd edition* (pp. 339-351). Cambridge, MA: MIT Press.
- 1086 Afifi, M., Barron, J. T., LeGendre, C., Tsai, Y.-T., & Bleibel, F. (2021). *Cross-camera*
1087 *convolutional color constancy*. Presented at the Proceedings of the IEEE/CVF
1088 International Conference on Computer Vision,
- 1089 Allred, S. R., & Brainard, D. H. (2013). A Bayesian model of lightness perception that
1090 incorporates spatial variation in the illumination. *Journal of Vision*, 13(7), 1-18.
- 1091 Alvaro, L., Linhares, J. M. M., Moreira, H., Lillo, J., & Nascimento, S. M. C. (2017). Robust
1092 colour constancy in red-green dichromats. *PLoS ONE*, 12(6), e0180310.
- 1093 American Society for Testing and Materials. (2017). Standard test method for luminous
1094 reflectance factor of acoustical materials by use of integrating-sphere reflectometers.
1095 *Renovations of Center for Historic Preservation*, 98(A), E1477.
- 1096 Arend, L., & Reeves, A. (1986). Simultaneous color constancy. *Journal Of The Optical Society*
1097 *Of America A*, 3(10), 1743-1751.
- 1098 Aston, S., Radonjić, A., Brainard, D. H., & Hurlbert, A. C. (2019). Illumination discrimination
1099 for chromatically biased illuminations: implications for colour constancy. *Journal of*
1100 *Vision*, 19(30:15)
- 1101 Banks, M. S., Geisler, W. S., & Bennett, P. J. (1987). The physical limits of grating visibility.
1102 *Vision Research*, 27(11), 1915-1924.
- 1103 Barron, J. T., & Malik, J. (2012a). *Color constancy, intrinsic images, and shape estimation*.
1104 Paper presented at ECCV.
- 1105 Barron, J. T., & Malik, J. (2012b). *Shape, albedo, and illumination from a single image of an*
1106 *unknown object*. Paper presented at IEEE Conference on Computer Vision and Pattern
1107 Recognition, 334-341.
- 1108 Bloj, M., Ripamonti, C., Mitha, K., Greenwald, S., Hauck, R., & Brainard, D. H. (2004). An
1109 equivalent illuminant model for the effect of surface slant on perceived lightness. *Journal*
1110 *of Vision*, 4(9), 735-746.
- 1111 Boyaci, H., Maloney, L. T., & Hersh, S. (2003). The effect of perceived surface orientation on
1112 perceived surface albedo in binocularly viewed scenes. *Journal of Vision*, 3(8), 541-553.
- 1113 Brainard, D. H. (1989). Calibration of a computer controlled color monitor. *Color Research &*
1114 *Application*, 14(1), 23-34.
- 1115 Brainard, D. H. (1998). Color constancy in the nearly natural image. 2. achromatic loci. *Journal*
1116 *of the Optical Society of America A*, 15(2), 307-325.
- 1117 Brainard, D. H. (2015). Color and the cone mosaic. *Annual Review of Vision Science*, 1, 519-
1118 546.
- 1119 Brainard, D. H., Brunt, W. A., & Speigle, J. M. (1997). Color constancy in the nearly natural
1120 image. 1. asymmetric matches. *Journal of the Optical Society of America A*, 14(9), 2091-
1121 2110.
- 1122 Brainard, D. H., & Freeman, W. T. (1997). Bayesian color constancy. *Journal of the Optical*
1123 *Society of America A*, 14(7), 1393-1411.

- 1124 Brainard, D. H., Longere, P., Delahunt, P. B., Freeman, W. T., Kraft, J. M., & Xiao, B. (2006).
1125 Bayesian model of human color constancy. *Journal of Vision*, 6(11), 1267-1281.
- 1126 Brainard, D. H., & Maloney, L. T. (2011). Surface color perception and equivalent illumination
1127 models. *Journal of Vision*, 11(5)
- 1128 Brainard, D. H., Pelli, D. G., & Robson, T. (2002). Display characterization. In J. P. Hornak
1129 (Ed.), *Encyclopedia of Imaging Science and Technology* (pp. 172-188). New York: Wiley.
- 1130 Brainard, D. H., & Radonjić, A. (2014). Color constancy. *The New Visual Neurosciences*, 1,
1131 545–556.
- 1132 Brascamp, J. W., & Shevell, S. K. (2021). The certainty of ambiguity in visual neural
1133 representations. *Annual Review of Vision Science*, in press
- 1134 Brindley, G. S. (1960). *Physiology of the Retina and the Visual Pathway*. London: Arnold.
- 1135 Brown, R. O., & MacLeod, D. I. A. (1997). Color appearance depends on the variance of
1136 surround colors. *Current Biology*, 7, 844-849.
- 1137 Burge, J. (2020). Image-computable ideal observers for tasks with natural stimuli. *Annual
1138 Review of Neuroscience*, 6, 491-517.
- 1139 Burge, J., & Geisler, W. S. (2011). Optimal defocus estimation in individual natural images.
1140 *Proceedings of the National Academy of Sciences*, 108(40), 16849-16854.
- 1141 Burge, J., & Geisler, W. S. (2014). Optimal disparity estimation in natural stereo images. *Journal
1142 of Vision*, 14(2)
- 1143 Burge, J., & Geisler, W. S. (2015). Optimal speed estimation in natural image movies predicts
1144 human performance. *Nature Communications*, 6, 7900.
- 1145 Burge, J., & Jaini, P. (2017). Accuracy maximization analysis for sensory-perceptual tasks:
1146 computational improvements, filter robustness, and coding advantages for scaled additive
1147 noise. *PLoS Computational Biology*, 13(2), e1005281.
- 1148 Burnham, R. W., Evans, R. M., & Newhall, S. M. (1952). Influence on color perception of
1149 adaptation to illumination. *Journal of the Optical Society of America*, 42(9), 597-605.
- 1150 Chichilnisky, E. J., & Wandell, B. A. (1997). Increment-decrement asymmetry in adaptation.
1151 *Vision Research*, 37, 616.
- 1152 Chin, B. M., & Burge, J. (2020). Predicting the partition of behavioral variability in speed
1153 perception with naturalistic stimuli. *Journal of Neuroscience*, 40(4), 864-879.
- 1154 CIE. (2007). *Fundamental chromaticity diagram with physiological axes – Parts 1 and 2.*
1155 *Technical Report 170-1*. Vienna: Central Bureau of the Commission Internationale de l'
1156 Éclairage.
- 1157 Cohen, J. (1964). Dependency of the spectral reflectance curves of the Munsell color chips.
1158 *Psychon. Sci.*, 1, 369-370.
- 1159 Cohen, M. R., & Newsome, W. T. (2009). Estimates of the contribution of single neurons to
1160 perception depend on timescale and noise correlation. *J Neurosci*, 29(20), 6635-6648.
- 1161 Cottaris, N. P., Jiang, H., Ding, X., Wandell, B. A., & Brainard, D. H. (2019). A computational-
1162 observer model of spatial contrast sensitivity: Effects of wave-front-based optics, cone-
1163 mosaic structure, and inference engine. *Journal of Vision*, 19(4), 8.
- 1164 Fechner, G. T. (1860). *Elements of Psychophysics* (H. E. Adler, 1966, Trans.). New York: Holt,
1165 Rinehart and Winston.
- 1166 Flachot, A., & Gegenfurtner, K. R. (2018). Processing of chromatic information in a deep
1167 convolutional neural network. *JOSA A*, 35(4), B334-B346.

- 1168 Flachot, A., & Gegenfurtner, K. R. (2021). Color for object recognition: Hue and chroma
1169 sensitivity in the deep features of convolutional neural networks. *Vision Research*, 182,
1170 89-100.
- 1171 Foster, D. H. (2011). Color constancy. *Vision Research*, 51(7), 674-700.
- 1172 Gegenfurtner, K., & Kiper, D. C. (1992). Contrast detection in luminance and chromatic noise.
1173 *Journal of the Optical Society of America A*, 9(11), 1880-1888.
- 1174 Gehler, P., Rother, C., Kiefel, M., Zhang, L., & Schölkopf, B. (2011). *Recovering intrinsic*
1175 *images with a global sparsity prior on reflectance*. Paper presented at Advances in
1176 Neural Information Processing Systems, 765-773.
- 1177 Geisler, W. S. (2008). Visual perception and the statistical properties of natural scenes. *Annual*
1178 *Review of Psychology*, 59, 167-192.
- 1179 Geisler, W. S., Najemnik, J., & Ing, A. D. (2009). Optimal stimulus encoders for natural tasks.
1180 *Journal of Vision*, 9(13), 17 11-16.
- 1181 Gilchrist, A. L. (1977). Perceived lightness depends on perceived spatial arrangement. *Science*,
1182 195, 185.
- 1183 Gilchrist, A. L. (2006). *Seeing Black and White*. Oxford: Oxford University Press.
- 1184 Giulianini, F., & Eskew, R. T., Jr. (1998). Chromatic masking in the (DL/L, DM/M) plane of
1185 cone-contrast space reveals only two detection mechanisms. *Vision Research*, 38, 3913-
1186 3926.
- 1187 Green, D. M., & Swets, J. A. (1966). *Signal Detection Theory and Psychophysics* (Vol. 1). New
1188 York: Wiley.
- 1189 Heasly, B. S., Cottaris, N. P., Lichtman, D. P., Xiao, B., & Brainard, D. H. (2014).
1190 RenderToolbox3: MATLAB tools that facilitate physically based stimulus rendering for
1191 vision research. *Journal of Vision*, 14(2)
- 1192 Helmholtz, H. (1896). *Physiological Optics*. New York: Dover Publications, Inc.
- 1193 Helson, H., & Jeffers, V. B. (1940). Fundamental problems in color vision. II. Hue, lightness,
1194 and saturation of selective samples in chromatic illumination. *Journal of Experimental*
1195 *Psychology*, 26(1), 1-27.
- 1196 Helson, H., & Michels, W. C. (1948). The effect of chromatic adaptation on achromaticity.
1197 *Journal of the Optical Society of America*, 38, 1025-1032.
- 1198 Henning, G. B., Hertz, B. G., & Hinton, J. L. (1981). Effects of different hypothetical detection
1199 mechanisms on the shape of spatial-frequency filters inferred from masking experiments:
1200 I. Noise masks. *Journal of the Optical Society of America*, 71(5), 574-581.
- 1201 Hillis, J. M., & Brainard, D. H. (2005). Do common mechanisms of adaptation mediate color
1202 discrimination and appearance? Uniform backgrounds. *Journal of the Optical Society of*
1203 *America A*, 22(10), 2090-2106.
- 1204 Hillis, J. M., & Brainard, D. H. (2007a). Distinct mechanisms mediate visual detection and
1205 identification. *Current Biology*, 17(19), 1714-1719.
- 1206 Hillis, J. M., & Brainard, D. H. (2007b). Do common mechanisms of adaptation mediate color
1207 discrimination and appearance? Contrast adaptation. *Journal of the Optical Society of*
1208 *America A*, 24(8), 2122-2133.
- 1209 Horn, B. K. P. (1974). Determining lightness from an image. *Computer Vision, Graphics, and*
1210 *Image Processing*, 3, 277-299.
- 1211 Hurlbert, A. (2019). Challenges to color constancy in a contemporary light. *Current Opinion in*
1212 *Behavioral Sciences*, 30:186, 186-193.
- 1213 Ishihara, S. (1977). Tests for colour-blindness. *Tokyo: Kanehara Shuppen Company, Ltd.*

- 1214 Jaini, P., & Burge, J. (2017). Linking normative models of natural tasks to descriptive models of
1215 neural response. *Journal of Vision*, 17(12), 16.
- 1216 Jakob, W. (2010). Mitsuba Renderer.
- 1217 Jameson, D., & Hurvich, L. M. (1955). Some quantitative aspects of an opponent-colors theory.
1218 I. Chromatic responses and spectral saturation. *Journal of the Optical Society of America*,
1219 45, 546-552.
- 1220 Jiang, H., Farrell, J., & Wandell, B. (2016). *A spectral estimation theory for color appearance*
1221 *matching*. Presented at the IS&T International Symposium on Electronic Imaging,
- 1222 Kelly, K. L., Gibson, K. S., & Nickerson, D. (1943). Tristimulus specification of the Munsell
1223 book of color from spectrophotometric measurements. *Journal of the Optical Society of*
1224 *America*, 33(7), 355-376.
- 1225 Kingdom, F. A. (2011). Lightness, brightness and transparency: a quarter century of new ideas,
1226 captivating demonstrations and unrelenting controversy. *Vision Research*, 51(7), 652-
1227 673.
- 1228 Knill, D. C., & Richards, W. (1996). *Perception as Bayesian Inference*. Cambridge: Cambridge
1229 University Press.
- 1230 Kraft, J. M., Maloney, S. I., & Brainard, D. H. (2002). Surface-illuminant ambiguity and color
1231 constancy: effects of scene complexity and depth cues. *Perception*, 31, 247-263.
- 1232 Land, E. H., & McCann, J. J. (1971). Lightness and retinex theory. *Journal of the Optical Society*
1233 *of America*, 61(1), 1-11.
- 1234 Legge, G. E., Kersten, D., & Burgess, A. E. (1987). Contrast discrimination in noise. *Journal of*
1235 *the Optical Society of America A*, 4(2), 391-404.
- 1236 Losada, M. A., & Mullen, K. T. (1995). Color and luminance spatial tuning estimated by noise
1237 masking in the absence of off-frequency looking. *Journal of the Optical Society of*
1238 *America A*, 12(2), 250-260.
- 1239 Lotto, R. B., & Purves, D. (1999). The effects of color on brightness. *Nature Neuroscience*,
1240 2(11), 1010-1014.
- 1241 Maloney, L. T. (1986). Evaluation of linear models of surface spectral reflectance with small
1242 numbers of parameters. *Journal Of The Optical Society Of America A*, 3(10), 1673-1683.
- 1243 Maloney, L. T., & Yang, J. N. (2001). The illuminant estimation hypothesis and surface color
1244 perception. In R. Mausfeld & D. Heyer (Eds.), *Colour Perception: From Light to Object*
1245 (pp. 335-358). Oxford: Oxford University Press.
- 1246 Marimont, D. H., & Wandell, B. A. (1994). Matching color images: the effects of axial
1247 chromatic aberration. *Journal of the Optical Society of America A*, 11(12), 3113-3122.
- 1248 Monaci, G., Menegaz, G., Süssstrunk, S., & Knoblauch, K. (2004). Chromatic contrast detection
1249 in spatial chromatic noise. *Visual Neuroscience*, 21, 291-294.
- 1250 Morimoto, T., & Smithson, H. E. (2018). Discrimination of spectral reflectance under
1251 environmental illumination. *J Opt Soc Am A Opt Image Sci Vis*, 35(4), B244-B255.
- 1252 Murray, R. F. (2020). A model of lightness perception guided by probabilistic assumptions about
1253 lighting and reflectance. *J Vis*, 20(7), 28.
- 1254 Murray, R. F. (2021). Lightness perception in complex scenes. *Annual Review of Vision Science*,
1255 7, 417-436.
- 1256 Nachmias, J. (1999). How is a grating detected on a narrowband noise masker? *Vision Research*,
1257 39(6), 1133-1142.
- 1258 Nachmias, J., & Sansbury, R. V. (1974). Grating contrast: discrimination may be better than
1259 detection. *Vision Research*, 14(10), 1039-1042.

- 1260 Nienborg, H., Cohen, M. R., & Cumming, B. G. (2012). Decision-related activity in sensory
1261 neurons: correlations among neurons and with behavior. *Annu Rev Neurosci*, 35, 463-
1262 483.
- 1263 Olkkonen, M., Witzel, C., Hansen, T., & Gegenfurtner, K. T. (2010). Categorical color
1264 constancy for real surfaces
. *Journal of Vision*, 10(9)
- 1265 Parker, A. J., & Newsome, W. T. (1998). Sense and the single neuron: probing the physiology of
1266 perception. *Annual Review of Neuroscience*, 21(1), 227-277.
- 1267 Parkkinen, J. P. S., Hallikainen, J., & Jaaskelainen, T. (1989). Characteristic spectra of Munsell
1268 colors. *Journal of the Optical Society of America*, 6(2), 318-322.
- 1269 Pearce, B., Crichton, S., Mackiewicz, M., Finlayson, G. D., & Hurlbert, A. (2014). Chromatic
1270 illumination discrimination ability reveals that human colour constancy is optimised for
1271 blue daylight illuminations. *PLoS ONE* 9(2:e87989), e87989.
- 1272 Pelli, D. G. (1990). The quantum efficiency of vision. In C. Blakemore (Ed.), *Vision: Coding
1273 and Efficiency* (pp. 3-24).
- 1274 Pelli, D. G., & Farell, B. (1999). Why use noise? *Journal of the Optical Society of America A*,
1275 16(3), 647-653.
- 1276 Prins, N., & Kingdom, F. A. A. (2018). Applying the model-comparison approach to test specific
1277 research hypotheses in psychophysical research using the Palamedes toolbox. *Frontiers
1278 in Psychology*, 9, 1250.
- 1279 Radonjić, A., & Brainard, D. H. (2016). The nature of instructional effects in color constancy. *J
1280 Exp Psychol Hum Percept Perform*, 42(6), 847-865.
- 1281 Radonjić, A., Cottaris, N. P., & Brainard, D. H. (2015). Color constancy supports cross-
1282 illumination color selection. *Journal of Vision*, 15(6), 1-19.
- 1283 Radonjić, A., Ding, X., Krieger, A., Aston, S., Hurlbert, A. C., & Brainard, D. H. (2018).
1284 Illumination discrimination in the absence of a fixed surface-reflectance layout. *Journal
1285 of Vision*, 18(5:11)
- 1286 Radonjić, A., & Gilchrist, A. L. (2013). Depth effect on lightness revisited: the role of
1287 articulation, proximity and fields of illumination. *i-Perception*, 4(6), 437-455.
- 1288 Radonjić, A., Pearce, B., Aston, S., Krieger, A., Dubin, H., Cottaris, N. P., Brainard, D. H., &
1289 Hurlbert, A. C. (2016). Illumination discrimination in real and simulated scenes. *Journal
1290 of Vision*, 16(11:2), 1-18.
- 1291 Rodieck, R. W. (1998). *The First Steps in Seeing*. Sunderland, Mass.: Sinauer.
- 1292 Rovamo, J., Franssila, R., & Nasanen, R. (1992). Contrast sensitivity as a function of spatial
1293 frequency, viewing distance and eccentricity with and without spatial noise. *Vision
1294 Research*, 32(4), 631-637.
- 1295 Rovamo, J., Raninen, A., & Donner, K. (1999). The effects of temporal noise and retinal
1296 luminance on foveal flicker sensitivity. *Vision Research*, 39, 533-539.
- 1297 Ruff, D. A., Ni, A. M., & Cohen, M. R. (2018). Cognition as a window into neuronal population
1298 space. *Annual Review of Neuroscience*, 41, 77-97.
- 1299 Sankeralli, M. J., & Mullen, K. T. (1997). Postreceptor chromatic detection mechanisms
1300 revealed by noise masking in three-dimensional cone contrast space. *Journal of the
1301 Optical Society of America A*, 14(10), 2633-2646.
- 1302 Schultz, S., Doerschner, K., & Maloney, L. T. (2006). Color constancy and hue scaling. *J Vis*,
1303 6(10), 1102-1116.
- 1304

- 1305 Shadlen, M. N., Britten, K. H., Newsome, W. T., & Movshon, J. A. (1996). A computational
1306 analysis of the relationship between neuronal and behavioral responses to visual motion.
1307 *Journal of Neuroscience*, 16, 1486-1510.
- 1308 Shen, L., & Yeo, C. (2011). *Intrinsic images decomposition using a local and global sparse*
1309 *representation of reflectance*. Presented at the IEEE Conference on Computer Vision and
1310 Pattern Recognition,
- 1311 Singh, V., Cottaris, N. P., Heasly, B. S., Brainard, D. H., & Burge, J. (2018). Computational
1312 luminance constancy from naturalistic images. *Journal of Vision*, 18(13), 19.
- 1313 Smithson, H. E. (2005). Sensory, computational, and cognitive components of human color
1314 constancy. *Philosophical Transactions of the Royal Society of London. Series B*,
1315 360(1458), 1329-1346.
- 1316 Teller, D. Y. (1984). Linking propositions. *Vision Research*, 24(10), 1233-1246.
- 1317 Thibos, L. N., Hong, X., Bradley, A., & Cheng, X. (2002). Statistical variation of aberration
1318 structure and image quality in a normal population of healthy eyes. *Journal of the Optical
1319 Society of America A*, 19(12), 2329-2348.
- 1320 von Kries, J. (1905). Influence of adaptation on the effects produced by luminous stimuli. In D.
1321 L. MacAdam (Ed.), *Sources of Color Science (1970)* (pp. 120-1126). Cambridge, MA:
1322 MIT Press.
- 1323 Vrhel, M. J., Gershon, R., & Iwan, L. S. (1994). Measurement and analysis of object reflectance
1324 spectra. *Color Research & Application*, 19(1), 4-9.
- 1325 Wandell, B. A., & Brainard, D. H. (in press). Principles and consequences of the initial visual
1326 encoding. In F. G. Ashby, H. Colonius & E. Dzhafarov (Eds.), *The New Handbook of
1327 Mathematical Psychology* Cambridge: Cambridge University Press.
- 1328 Webster, M. A., & Mollon, J. D. (1995). Colour constancy influenced by contrast adaptation.
1329 *Nature*, 373(6516), 694-698.
- 1330 Weiss, D., Witzel, C., & Gegenfurtner, K. (2017). Determinants of colour constancy and the blue
1331 bias. *i-Perception*, 8(6), 204166951773963.
- 1332 Whittle, P., & Challands, P. D. C. (1969). The effect of background luminance on the brightness
1333 of flashes. *Vision Research*, 9(9), 1095-1110.
- 1334 Witzel, C., & Gegenfurtner, K. R. (2018). Color perception: objects, constancy, and categories.
1335 *Annual Review of Vision Science*, 4, 475-499.
- 1336 Yang, J. N., & Maloney, L. T. (2001). Illuminant cues in surface color perception: tests of three
1337 candidate cues. *Vision Research*, 41, 2581-2600.
- 1338 Zhang, X., & Brainard, D. H. (2004). *Bayesian color correction method for non-colorimetric*
1339 *digital image sensors*. Paper presented at Color and Imaging Conference, 308-314.
- 1340 Zhu, H., Yuille, A., & Kersten, D. (2021). *Three-dimensional pose discrimination in natural*
1341 *images of humans*. Presented at the Annual Meeting of the Vision Sciences Society, May
1342 21-26, 2021. Poster A70.
- 1343